



This is a repository copy of *Reconstruction of the Greenland Ice Sheet surface mass balance and the spatiotemporal distribution of freshwater runoff from Greenland to surrounding seas*.

White Rose Research Online URL for this paper:
<http://eprints.whiterose.ac.uk/142136/>

Version: Submitted Version

Article:

Mernild, S.H., Liston, G.E., Beckerman, A.P. et al. (1 more author) (Submitted: 2017)
Reconstruction of the Greenland Ice Sheet surface mass balance and the spatiotemporal distribution of freshwater runoff from Greenland to surrounding seas. *The Cryosphere*. ISSN 1994-0416 (Submitted)

<https://doi.org/10.5194/tc-2017-234>

Reuse

This article is distributed under the terms of the Creative Commons Attribution (CC BY) licence. This licence allows you to distribute, remix, tweak, and build upon the work, even commercially, as long as you credit the authors for the original work. More information and the full terms of the licence here:
<https://creativecommons.org/licenses/>

Takedown

If you consider content in White Rose Research Online to be in breach of UK law, please notify us by emailing eprints@whiterose.ac.uk including the URL of the record and the reason for the withdrawal request.



eprints@whiterose.ac.uk
<https://eprints.whiterose.ac.uk/>



26 **Abstract**

27 Knowledge about variations in runoff from Greenland to adjacent fjords and seas is important for
28 the hydrochemistry and ocean research communities to understand the link between terrestrial
29 and marine Arctic environments. Here, we simulate the Greenland Ice Sheet (GrIS) surface mass
30 balance (SMB), including refreezing and retention, and runoff together with catchment-scale
31 runoff from the entire Greenland landmass ($n = 3,272$ simulated catchments) throughout the 35-
32 year period 1979–2014. SnowModel/HydroFlow was applied at 3-h intervals to resolve the
33 diurnal cycle and at 5-km horizontal grid increments using ERA-Interim (ERA-I) reanalysis
34 atmospheric forcing. Simulated SMB was low compared to earlier studies, whereas the GrIS
35 surface conditions and precipitation were similar. Variations in meteorological and surface ice
36 and snow cover conditions influenced the seasonal variability in simulated catchment runoff;
37 variations in the GrIS internal drainage system were assumed negligible and a time-invariant
38 digital elevation model was applied. Approximately 80 % of all catchments showed increasing
39 runoff trends over the 35 years, with on average relatively high and low catchment-scale runoff
40 from the SW and N parts of Greenland, respectively. Outputs from an Empirical Orthogonal
41 Function (EOF) analysis were combined with cross-correlations indicating a direct link (zero lag
42 time) between modeled catchment-scale runoff and variations in the large-scale atmospheric
43 circulation indices North Atlantic Oscillation (NAO) and Atlantic Multidecadal Oscillation
44 (AMO). This suggests that natural variabilities in AMO and NAO constitute major controls on
45 catchment-scale runoff variations in Greenland.

46

47 **KEYWORDS:** Empirical Orthogonal Function; Greenland freshwater runoff; Greenland Ice
48 Sheet; HydroFlow; Modeling; NASA MERRA; SnowModel; surface mass-balance



49 1. Introduction

50 The Greenland Ice Sheet (GrIS) is highly sensitive to changes in climate (e.g., Box et al.
51 2012; Hanna et al. 2013; Langen et al. 2015; Wilton et al. 2016; AMAP 2017). It is of scientific
52 interest and importance because it constitutes a massive reserve of freshwater that discharges to
53 adjacent fjords and seas (Cullather et al. 2016). Runoff from Greenland influences the sea
54 surface temperature, salinity, stratification, marine ecology, and sea-level in a number of direct
55 and indirect ways (e.g., Rahmstorf et al. 2005; Straneo et al. 2011; Shepherd et al. 2012; Weijer
56 et al. 2012; Church et al. 2013; Lenaerts et al. 2015).

57 The GrIS surface mass balance (SMB) and freshwater runoff have changed over the last
58 decades and most significantly since the mid-1990s (e.g., Church et al. 2013; Wilton et al. 2016).
59 For example, recent estimates by Wilton et al. (2016) showed a decrease in SMB from ~350 Gt
60 yr^{-1} (early-1990s) to ~100 Gt yr^{-1} (late-2000s) and an increase in runoff from ~200 Gt yr^{-1} (early-
61 1990s) to ~450 Gt yr^{-1} (late-2000s). For 2009 through 2012, the runoff has been estimated to
62 include approximately two-third of the gross GrIS mass loss (Enderlin et al. 2014), while the net
63 GrIS mass loss, on average, was 375 Gt yr^{-1} (2011–2014) (AMAP 2017). The contribution of
64 GrIS mass loss to global mean sea-level was around 5 % in 1993, and more than 25 % in 2014
65 (Chen et al. 2017). Noël et al. (2017), however, estimated the GrIS and peripheral glaciers to
66 contribute approximately 43 % to the contemporary sea-level rise.

67 Runoff from the GrIS is an integrated response of rain, snowmelt, and glacier melt and
68 other hydrometeorological processes (e.g., Bliss et al. 2014). Tedesco et al. (2016) estimated a
69 1979–2016 change in GrIS spatial surface melt extent of ~15,820 $\text{km}^2 \text{yr}^{-1}$, and a change in
70 surface ablation duration of ~30–40 days in NE and 15–20 days along the west coast. At higher
71 GrIS elevations, surface melt does not necessarily equal surface runoff because meltwater may



72 refreeze in the porous near-surface snow and firn layers (Machguth et al. 2016) where the firn
73 pore space provides potential storage for meltwater (Haper et al. 2012; van Angelen et al. 2013).
74 Melt water percolation, refreezing, and densification processes are common in GrIS snow, firn,
75 and multi-year firn layers – especially where semipermeable or impermeable ice layers are
76 present (Brown et al. 2012; van As et al. 2016). Such physical mechanisms and conditions in the
77 firn and multi-year firn layers lead, e.g., to non-linearity in meltwater retention (Brown et al. 2012).

78 The GrIS internal drainage system has received increased attention in recent years. This
79 is, in part, because the summer acceleration of ice flow is controlled by supraglacial meltwater
80 draining to the subglacial environment (Zwally et al. 2002; van de Wal et al. 2008; Shephard et
81 al. 2009). Enhanced production of supraglacial meltwater results in more water supplied to the
82 glacier bed, leading to reduced basal drag and accelerated basal ice motion. This process is
83 referred to as basal lubrication, and it constitutes a potential positive feedback mechanism
84 between climate change and sea-level rise (Hewitt 2013). At high GrIS elevations, surface
85 meltwater primarily drains to the glacier bed via hydrofractures (van der Veen 2007), whereas
86 meltwater is routed to the glacier bed via crevasses and moulins in the peripheral areas (Banwell
87 et al. 2016; Everett et al. 2016; Koziol et al. 2017). Rapid drainage of large volumes of GrIS
88 meltwater come from sudden release from supraglacial and proglacial lakes (known as a glacial
89 lake outburst flood (GLOF) or jökulhlaup), which are particular common in West Greenland
90 (Selmes et al. 2011; Carrivick and Quincey 2014). The seasonal evolution of the structure and
91 efficiency of the drainage system beneath the GrIS is indirectly assumed from our understanding
92 of the subglacial hydraulic potential beneath Alpine glaciers. This general understanding is used
93 explain the observed seasonal changes in ice motion (Bartholomew et al. 2010, 2012) where few
94 direct observations exist (Kohler et al. 2017). In fact, we know very little about spatiotemporal



95 shifts in the configuration of the subglacial drainage network beneath the GrIS. We therefore
96 assume that the subglacial drainage network in the natural system is dynamic and sensitive to
97 rerouting of water flow between adjacent catchments (so-called water piracy; Chu et al. 2016),
98 although we do not understand the details sufficiently to implement them in a runoff routing
99 model.

100 We also lack high resolution information on the spatiotemporal distribution of GrIS and
101 Greenland freshwater runoff to the fjords and seas, and the spatiotemporal distribution of solid-
102 ice discharge (calving) from tidewater glaciers is also largely unknown (Howat et al. 2013). To
103 address this lack of knowledge, information about the quantitative discharge (runoff and solid-
104 ice discharge) conditions from the numerous of catchments in Greenland is required. Available
105 GrIS calving rates are insufficient to represent the calving rates from the entire Greenland and
106 are therefore not generally included in overall Greenland freshwater estimates (Nick et al. 2009;
107 Lenaerts et al. 2015). This is an unaddressed gap, which likely prevents us from
108 comprehensively understanding the terrestrial freshwater discharge to the fjords and seas. This
109 also limits the subsequent the link between changes in terrestrial inputs and changes in the
110 hydrographic and circulation conditions. This unaddressed knowledge gap has further
111 implications for ocean model simulations, where, for example, earlier representations of
112 Greenland discharge boundary conditions were either non-existent or overly simplistic (e.g.,
113 Weijer et al. 2012).

114 Previous GrIS studies constructed a section-wise runoff distribution by dividing the ice
115 sheet into six to eight overall defined sections (e.g., Rignot et al. 2008; Bamber et al. 2012;
116 Rignot and Mouginot 2012; Lenaerts et al. 2015; Wilton et al. 2016). These studies illustrated an



117 increase in runoff since 1870 for all GrIS sections, with the greatest increase in runoff since mid-
118 1990s and in the SW part of the ice sheet.

119 Mernild and Liston (2012) reconstructed the GrIS SMB and the Greenland
120 spatiotemporal runoff distribution from ~3,150 individually simulated catchments, at 5-km
121 spatial, and daily temporal, resolutions covering the period from 1960 through 2010. Automatic
122 weather stations located both on and off the GrIS were used for atmospheric forcings, and the
123 study was carried out using a full energy balance, multi-layer snowpack and snow distribution,
124 and freshwater runoff model and software package called SnowModel/HydroFlow (Liston and
125 Elder 2006a; Liston and Mernild 2012). These individual catchment outlet runoff time series
126 were analyzed to map runoff magnitudes and variabilities in time, but also emphasized trends
127 and spatiotemporal variations, including runoff contributions from the GrIS, the land area
128 between the GrIS ice margin and the ocean, from the relatively small isolated glaciers and ice
129 caps, and from entire Greenland. This approach is especially important when trying to
130 understand the total runoff fraction from Greenland, including the annual and seasonal
131 freshwater runoff variabilities within individual catchments.

132 Here, we improve the work by Mernild and Liston (2012) by using an updated version of
133 SnowModel/HydroFlow and by including a new digital elevation model (DEM). We also extend
134 the time series to 2014 by using the ERA-Interim (ERA-I) reanalysis products on 3-h time step
135 (Dee et al. 2011). The objective of this study is to simulate, map, and analyze first-order
136 atmospheric forcings and GrIS mass balance components for Greenland. The analyzed variables
137 include the GrIS SMB, together with GrIS surface air temperature, surface melt, precipitation,
138 evaporation, sublimation, refreezing and retention, and surface freshwater runoff and specific
139 runoff (runoff volume per time per unit drainage area, $L s^{-1} km^{-2}$; to convert to $mm yr^{-1}$, multiply



140 by 31.6) conditions. The time period covers 1979–2014 (35 years), with a focus on the present
141 day conditions 2005–2014 (the last decade of the simulations). Further, the spatiotemporal
142 magnitude, distribution, and trends of individual catchment-scale runoff and specific runoff from
143 Greenland ($n = 3,272$; where n is the number of simulated catchments, each with an individual
144 flow network) were simulated based on HydroFlow-generated watershed divides and flow
145 networks for each catchment. The simulated spatiotemporal catchment-scale outlet runoff is
146 useful as boundary conditions for fjord and ocean model simulations. We also analyzed the
147 spatiotemporal catchment-scale outlet runoff using Empirical Orthogonal Functions (EOF). This
148 analysis allowed us to describe simultaneously how the spatial patterns of catchment-scale outlet
149 runoff changed over time. It also allowed us to explore via cross-correlations the relationship
150 between the spatiotemporal patterns and large-scale atmospheric-ocean circulation indices
151 including the North Atlantic Oscillation (NAO) and the Atlantic Multidecadal Oscillation
152 (AMO), with particular attention to the lag-times, if any, between variations in NAO and AMO
153 and responses in Greenland catchment-scale runoff.

154

155 **2. Model description, setup, and verification**

156 2.1 SnowModel

157 SnowModel (Liston and Elder 2006a) is established by six sub-models, where five of the
158 models were used here to quantify spatiotemporal variations in atmospheric forcing, surface
159 snow properties, GrIS SMB, and Greenland catchment runoff. The sub-model MicroMet (Liston
160 and Elder 2006b; Mernild et al. 2006a) downscaled and distributed the spatiotemporal
161 atmospheric fields using the Barnes objective interpolation scheme, where the interpolated fields
162 subsequent were adjusted using known meteorological algorithms, e.g., temperature-elevation,



163 wind-topography, humidity-cloudiness, and radiation-cloud-topography relationships (Liston and
164 Elder 2006b). Enbal (Liston 1995; Liston et al. 1999) simulated a full surface energy balance
165 considering the influence of cloud cover, sun angle, topographic slope, and aspect on incoming
166 solar radiation, and moisture exchanges, e.g., multilayer heat- and mass-transfer processes within
167 the snow (Liston and Mernild 2012). SnowTran-3D (Liston and Sturm 1998, 2002; Liston et al.
168 2007) accounted for the snow (re)distribution by wind. SnowPack-ML (Liston and Mernild 2012)
169 simulated multilayer snow depths, temperatures, and water-equivalent evolutions. HydroFlow
170 (Liston and Mernild 2012) simulated watershed divides, routing network, flow residence-time,
171 and runoff routing (configurations based on the hypothetical gridded topography and ocean-mask
172 datasets), and discharge hydrographs for each grid cell including from catchment outlets. These
173 sub-models have been tested against independent observations with success in Greenland, Arctic,
174 high mountain regions, and on the Antarctic Ice Sheet with acceptable results (e.g., Hiemstra et
175 al. 2006; Liston and Hiemstra 2011; Beamer et al. 2016). For detailed information regarding the
176 use of SnowModel for the GrIS' or local Greenlandic glaciers' SMB and runoff simulations, we
177 refer to Mernild and Liston (2010, 2012) and Mernild et al. (2010a, 2014).

178

179 2.2 Meteorological forcing, model configuration and model limitations

180 SnowModel was forced with ERA-Interim (ERA-I) reanalysis products on a 0.75°
181 longitude \times 0.75° latitude grid from the European Centre for Medium-Range Weather Forecasts
182 (ECMWF; Dee et al. 2011). The simulations were conducted from 1 September 1979 through 31
183 August 2014 (35 years) (henceforth 1979–2014), where the 6-hour (precipitation at 12-hour)
184 temporal resolution ERA-I data was downscaled to 3-hourly values and a 5-km grid using
185 MicroMet. The 3-hour temporal resolution was chosen to allow SnowModel to resolve the solar



186 radiation diurnal cycle in its simulation of snow and ice temperature evolution and melt
187 processes.

188 The DEM was obtained from Levinsen et al. (2015), and rescaled to a 5-km horizontal
189 grid increment that covered the GrIS (1,646,175 km²), mountain glaciers, and the entire
190 Greenland (2,166,725 km²) and the surrounding fjords and seas (Figure 1a). The DEM is time-
191 invariant specific to the year 2010. The DEM was developed by merging contemporary radar and
192 laser altimetry data, where radar data were acquired with Envisat and CryoSat-2, and laser data
193 with the Ice, Cloud, and land Elevation Satellite (ICESat), the Airborne Topographic Mapper
194 (ATM), and the Land, Vegetation, and Ice Sensor (LVIS). Radar data were corrected for
195 horizontal, slope-induced, and vertical errors from penetration of the echoes into the subsurface
196 (Levinsen et al. 2015). Since laser data are not subject to such errors, merging radar and laser
197 data yields a DEM that resolves both surface depressions and topographic features at higher
198 altitudes (Levinsen et al. 2015). The distribution of glacier cover was obtained from the
199 Randolph Glacier Inventory (RGI, v. 5.0) polygons; these data were resampled to the 5-km grid.
200 The SnowModel land-cover mask defined glaciers to be present when individual grid cells were
201 covered by 50 % or more of glacier ice.

202 First, the GrIS DEM was initially divided into six major sections following Rignot et al.
203 (unpublished): southwest (SW), west (W), northwest (NW), north (N), northeast (NE), and
204 southwest (SW) (Figure 1b and Table 1). Second, HydroFlow divided Greenland into 3,272
205 individual catchments (Figure 1c), each with an eight-compass-direction water-flow network
206 where water is transported through this network via linear reservoirs. Only a single outlet into the
207 seas was allowed for each individual catchment.



208 The mean and median catchment sizes were 680 km² and 75 km², respectively. The top
209 one percent of the largest catchments accounted for 53 % of the Greenland area. This distribution
210 of HydroFlow-defined GrIS catchments (Figure 1c) closely matched both the catchment
211 distribution by Mernild and Liston (2012) and by Rignot and Kanagaratnam (2006) for the 20
212 largest GrIS catchments (not including midsize and minor catchments), both with respect to size
213 and location of the watershed divide. The total number of HydroFlow-generated catchments
214 presented in this study was ~4 % higher than the number of Greenland catchments in the Mernild
215 and Liston (2012) study.

216 In MicroMet, only one-way atmospheric coupling was provided, where the
217 meteorological conditions were prescribed at each time step. In the natural system, the
218 atmospheric conditions would be adjusted in response to changes in surface conditions and
219 properties (Liston and Hiemstra 2011). Due to the use of the 5-km horizontal grid increments,
220 snow transport and blowing-snow sublimation processes (usually produced by SnowTran-3D in
221 SnowModel) were excluded from the simulations because blowing snow does not typically move
222 completely across 5-km distances. Static sublimation was, however, included in the model
223 integrations. In HydroFlow, the generated catchment divides and flow network were controlled
224 by the DEM, i.e., exclusively by the surface topography and not by the development of the
225 glacial drainage system. The role of GrIS bedrock topography on controlling the potentiometric
226 surface and the associated meltwater flow direction was assumed to be a secondary control on
227 discharge processes (Cuffey and Paterson 2010).

228 An example of the HydroFlow generated catchment divides and flow network is
229 illustrated in detail by Mernild et al. (2017; Figure 1c) for the Kangerlussuaq catchment in
230 central West Greenland, which includes a part of the GrIS (67°N, 50°W; SW sector of the GrIS).



231 Because the DEM is time-invariant, no changes though feedbacks from a thinning ice, ice retreat,
232 and from changes in hypsometry will influence the catchment divides and the flow network
233 patterns, including the glacial drainage system. Changes in runoff over time are therefore solely
234 influenced by the climate signal and the surface snow and ice cover conditions (runoff was
235 generated from gridded inputs from rain, snowmelt, and ice melt), not by the glacial drainage
236 system. In HydroFlow, the meltwater flow velocities were gained from dye tracer experiments
237 conducted both through the snowpack (in early and late-summer) and through the englacial and
238 subglacial environments (Mernild et al. 2006b).

239

240 2.3 Verification

241 For Greenland, long-term catchment river runoff observations are sparse; at present
242 approximately ten permanent hydrometric monitoring stations are operating, measuring the sub-
243 daily and sub-seasonal runoff variability originating from rain, melting snow, and melting ice
244 from local glaciers and the GrIS. In addition, these observations only span parts of the runoff
245 season, ranging between few weeks to approximately three months. For the Kangerlussuaq area,
246 independent meteorological and snow and ice observational datasets are also available, e.g., K-
247 transect point observed air temperature and SMB and catchment outlet observed discharge (e.g.,
248 van de Wal et al. 2005; van den Broeke et al. 2008a; 2008b, Hasholt et. al. 2013). These
249 observed datasets were used for verification of the SnowModel/HydroFlow ERA-I simulated
250 GrIS mean annual air temperature (MAAT), GrIS SMB, and catchment freshwater runoff
251 presented herein (Mernild et al. 2017). These model verifications showed acceptable results (for
252 further information see Mernild et al. 2017). The use of ERA-I has also showed promising



253 results after a full evaluation estimating changes in ice sheet surface mass balance for the
254 catchments linked to Godthåbsfjord (64° N) in Southwest Greenland (Langen et al. 2015).

255 In the analysis that follows, all correlation trends declared ‘significant’ are statistically
256 significant at or above the 5 % level ($p < 0.05$; based on a linear regression t test).

257

258 2.4 Surface water balance components

259 For the GrIS, surface water balance components can be estimated using the hydrological
260 method (continuity equation) (Equation 1):

261

$$262 \quad P - (Su + E) - R + \Delta S = 0 \pm \eta, \quad (1)$$

263

264 where P is precipitation input from snow and rain, Su is sublimation from a static surface, E is
265 evaporation, R is runoff from snowmelt, ice melt, and rain, ΔS is change in storage (ΔS is also
266 referred to as SMB) derived as the residual value from changes in glacier and snowpack storage.

267 For snow and ice surfaces, the ablation was estimated as: $Su + E + R$. The amount of snow
268 refreezing and retention was estimated as: $P_{\text{rain}} + \text{melt}_{\text{surface}} - R$ (for bare ice: $P_{\text{rain}} + \text{melt}_{\text{surface}} =$
269 R). The parameter η is the water balance discrepancy. This discrepancy should be 0 (or small), if
270 the components P, Su, E, R, and ΔS have been determined accurately.

271

272 3. EOF runoff analysis

273 We applied an Empirical Orthogonal Function (EOF) analysis to define the
274 spatiotemporal pattern in simulated catchment outlet runoff. EOF is a statistical tool that
275 analyzes spatial and temporal runoff data to find combinations of locations that vary consistently



276 through time, and combinations of time, that vary in a spatially consistent manner (e.g.,
277 Preisendorfer 1998; Sparnocchia et al. 2003). The major axes of the EOF analysis identify
278 variations in the catchment outlet runoff in both time and space.

279 The eigenvalues of the EOFs can be correlated with the temporal data, and the
280 eigenvectors with spatial locations, to identify how the EOF describes change in runoff in time
281 and across space. Furthermore, the temporal patterns embedded in the EOFs can, via cross-
282 correlation analysis, be related to larger scale atmospheric-ocean indices (Mernild et al. 2015), in
283 this case the North Atlantic Oscillation (NAO) and Atlantic Multi-decadal Oscillation (AMO).
284 The NAO and AMO indices were obtained from Hurrell and van Loon (1997) and Kaplan et al.
285 (1998), respectively. This latter analysis can generate hypotheses about whether, for example,
286 NAO or AMO leads by some years changes in mass balance and runoff (the lag in the cross-
287 correlation analyses tells us these details).

288 We focused on the NAO and AMO for several reasons. NAO is estimated based on the
289 mean sea-level pressure difference between the Azores High and Icelandic Low. NAO is a large-
290 scale atmospheric circulation index, and is therefore a good measure of airflow and jet-stream
291 moisture transport variability (e.g., Overland et al. 2012) from the North Atlantic onto Northwest
292 Europe (Dickson et al. 2000; Rogers et al. 2001). According to Hurrell (1995), a positive NAO is
293 associated with cold conditions in Greenland, while a negative NAO corresponds to mild
294 conditions. AMO is a large-scale oceanic circulation index, and an expression of fluctuating
295 mean sea-surface temperatures in the North Atlantic (Kaplan et al. 1998). For example, Arctic
296 land surface air temperatures are highly correlated with the AMO (Chylek et al. 2010), and the
297 overall annual trend in the mean GrIS melt extent correlates with the smoothed trends of the
298 AMO (Mernild et al. 2011). A positive AMO indicates relatively high surface air temperature



299 and less precipitation at high latitudes (relatively high net mass balance loss), whereas a negative
300 AMO indicates relatively low surface air temperature and a higher precipitation (relatively low
301 net mass balance loss) (Kaplan et al. 1998).

302

303 **4. Results and discussion**

304 4.1 GrIS surface water balance conditions

305 Figure 2 presents the SnowModel ERA-I simulated 35-year mean spatial GrIS surface
306 MAAT, precipitation, surface melt, evaporation and sublimation, ablation, and SMB. Overall, all
307 variables follow the expected spatial patterns. For example, the lowest MAAT occurred at the
308 GrIS interior ($\leq -27^{\circ}\text{C}$) and highest values were at the margin ($\geq 0^{\circ}\text{C}$). Also, the lowest annual
309 mean precipitation values were situated in the northern half of the GrIS interior (≤ 0.25 m water
310 equivalent (w.e.)), while peak values occurred in the southeastern part of Greenland (≥ 3.5 m
311 w.e.). The lowest annual mean surface melt values (≤ 0.0625 m w.e.) were present at the upper
312 parts of the GrIS and vice versa at the lowest margin areas (≥ 5.0 m w.e.). The 35-year mean
313 SMB illustrated net loss at the lowest elevations of ≥ 4.0 m w.e. and net gain at the highest
314 elevations of between 0 and 0.25 m w.e. The peak net gain of ≥ 3.5 m w.e. occurred in Southeast
315 Greenland, which matches what is generally expected from the overall precipitation pattern over
316 the GrIS. The SnowModel ERA-I spatial simulated 35-year mean distributions generally agree
317 with previous studies by Fettweis et al. (2008, 2017), Hanna et al. (2011), and Box (2013),
318 within the different temporal domains covered by these studies.

319 On GrIS section-scale (Table 1), a clear variability between the six sections occurred for
320 the surface mass-balance components (Equation 1) for both the 35-year mean and the last
321 decade. On average, most precipitation fell in the Southeast Greenland sector of 242.6 ± 39.1 Gt



322 yr⁻¹ (where, ± equals one standard deviation). This was likely due to the cyclonicity between
323 Iceland and Greenland, which typically sets up a prevailing easterly airflow towards the
324 southeastern coast of Greenland that includes orographic enhancement (Hanna et al. 2006; Bales
325 et al. 2009). The lowest 35-year mean precipitation of 31.1 ± 5.4 Gt yr⁻¹ occurred in the dry
326 North Greenland. For the last decade, the mean annual precipitation was 232.4 ± 25.2 Gt yr⁻¹ and
327 30.9 ± 5.1 Gt yr⁻¹ for Southeast Greenland and North Greenland, respectively. This regional
328 distribution is in accordance with the study on Greenlandic precipitation patterns by Mernild et
329 al. (2015), although their analysis was based on observed precipitation from 2001–2012. Further,
330 in Mernild et al. (2017; Figure 6b), the mean ERA-I grid point precipitation (located closest to
331 the center of the Kangerlussuaq watershed) was tested against Kangerlussuaq SnowModel ERA-
332 I downscaled mean catchment precipitation conditions; this analysis indicated no significant
333 difference between the two datasets.

334 The ratio between rain and snow precipitation varied from <1 % (Northeast section) to 5
335 % (Southwest section), averaging 2 % and indicating that rain only played a minor role in the
336 GrIS precipitation budget (Table 1). For the last decade, the average rainfall-to-snowfall ratio
337 was 3 % for the entire GrIS.

338 For the GrIS, the overall precipitation was 653.9 ± 66.4 Gt yr⁻¹ (35 years) and $645.0 \pm$
339 39.0 Gt yr⁻¹ (2005–2014), which is within the lower range of previously reported values
340 (Fettweis et al. 2017; Table 1). For example, in MAR (Modèle Atmosphérique Régional; v.
341 3.5.2) the simulated precipitation was between 747.0–642.0 Gt yr⁻¹ (1980–1999; snowfall plus
342 rainfall) forced with a variety of forcings, e.g., ERA-40 (Uppala et al. 2005), ERA-I (Dee et al.
343 2011), JRA-55 (Japanese 55-year Reanalysis; Kobayashi et al. 2015).



344 As shown by Fettweis et al. (2017), precipitation is the parameter with the largest
345 uncertainty due to the spread among the different forcing datasets. Also, systematic observational
346 errors may occur during precipitation monitoring, such as wind-induced undercatch, because of
347 turbulence and wind field deformation from the precipitation gauge, wetting losses, and trace
348 amounts (e.g., Goodison et al. 1989; Metcalfe et al. 1994; Yang et al. 1999; Rasmussen et al.
349 2012). An understanding of precipitation conditions and uncertainties are therefore highly
350 relevant for estimating the energy and moisture balances, surface albedo, GrIS SMB conditions,
351 and, in a broader perspective, the GrIS's contribution to sea-level changes.

352 Besides precipitation, melt and ablation are other relevant parameters for estimation and
353 understanding GrIS surface conditions, where surface melt (including extent, intensity, and
354 duration) is relevant for SMB conditions. An altered surface melt regime can influence surface
355 albedo, because wet snow absorbs up to three times more incident solar energy than dry snow
356 (Steffen 1995), and the energy and moisture balances. Changes in the amount of meltwater also
357 affect total runoff, ice dynamics, and subglacial lubrication and sliding processes (Hewitt 2013).

358 Surface melt varied on a section-scale, for the 35-year mean, from 57.2 ± 24.1 Gt yr⁻¹ in
359 North Greenland to 155.2 ± 48.4 Gt yr⁻¹ in Southwest Greenland (Table 1). The average for the
360 entire GrIS was 542.9 ± 175.3 Gt yr⁻¹ (Table 1). During the last decade, the surface melt for the
361 GrIS had increased to 713.4 ± 138.6 Gt yr⁻¹, varying from 75.9 ± 26.9 Gt yr⁻¹ in Northeast
362 Greenland to 202.4 ± 39.2 Gt yr⁻¹ in Southwest Greenland. This is an increase of 31 % for the
363 last decade compared to the entire simulation period, which was likely due to increasing MAAT
364 (assuming an empirical relationship between air temperature (sensible heat) and surface melt
365 rates) throughout the simulation period (Hanna et al. 2012).



366 The GrIS ablation patterns varied as expected between the northern and southern sections
367 from $65.7 \pm 22.6 \text{ Gt yr}^{-1}$ in the north to $132.9 \pm 42.2 \text{ Gt yr}^{-1}$ in the south. For the entire GrIS, the
368 mean annual ablation was $530.3 \pm 153 \text{ Gt yr}^{-1}$ and $687.8 \pm 118.8 \text{ Gt yr}^{-1}$ for the 35-year period
369 and 2005–2014, respectively. This was equal to an increase of 30 %, which was also reflected in
370 the differences in variability from $83.3 \pm 24.7 \text{ Gt yr}^{-1}$ in North Greenland to $175.1 \pm 35.2 \text{ Gt yr}^{-1}$
371 in Southwest Greenland (Table 1).

372 Runoff is a part of the ablation budget and therefore must be quantified to understand
373 GrIS mass balance changes. Runoff varied from $50.0 \pm 22.7 \text{ Gt yr}^{-1}$ in North Greenland to 112.6
374 $\pm 41.8 \text{ Gt yr}^{-1}$ in South Greenland, averaging $418.1 \pm 151.1 \text{ Gt yr}^{-1}$ for the 35-year mean period.
375 For 2005–2014, the mean runoff was $73.7 \pm 119.8 \text{ Gt yr}^{-1}$; a 37 % increase (Table 1). This
376 increase confirms the results from previous studies (e.g., Wilton et al. 2016). On a regional-scale,
377 runoff varied from $67.6 \pm 25.0 \text{ Gt yr}^{-1}$ in North Greenland to $154.4 \pm 36.3 \text{ Gt yr}^{-1}$ in Southwest
378 Greenland. The simulated section runoff distribution was largely in agreement with trends noted
379 by Lewis and Smith (2009) and Mernild and Liston (2012). The section runoff variability
380 roughly followed the precipitation patterns, where sections with high precipitation equaled low
381 runoff (e.g., in Southeast Greenland) and vice versa (e.g., in Southwest Greenland). More
382 specifically, GrIS snowpack retention and refreezing processes suggest that sections with
383 relatively high surface runoff were synchronous with relatively low end-of-winter snow
384 accumulation because more meltwater was retained in the thicker, colder snowpack, reducing
385 and delaying runoff to the internal glacier drainage system (e.g., Hanna et al. 2008). However, in
386 maritime regions such as Southeast Greenland, high surface runoff can result from abnormally
387 wet conditions (Mernild et al. 2014). Furthermore, runoff was negatively correlated to surface
388 albedo and snow cold content, as confirmed by Hanna et al. (2008) and Ettema et al. (2009).



389 For the dry North and Northeast Greenland (Table 1), the relatively low end-of-winter
390 snowpack melted relatively fast during spring warm-up. After the winter snowpack had ablated,
391 the ice surface albedo promoted a stronger radiation-driven ablation and surface runoff, owing to
392 the lower ice albedo. For the wetter Southeast Greenland (Table 1), the relatively high end-of-
393 winter snow accumulation, combined with frequent summer snow precipitation events, kept the
394 albedo high. Therefore, in that region it generally took longer time to melt the snowpack
395 compared to the drier parts of the GrIS before ablation started to affect the underlying glacier ice.

396 Regarding specific runoff (runoff volume per unit drainage area per time, $\text{L s}^{-1} \text{ km}^{-2}$; to
397 convert to mm yr^{-1} , multiply by 31.6), maximum values of $16.7 \text{ L s}^{-1} \text{ km}^{-2}$ and $22.9 \text{ L s}^{-1} \text{ km}^{-2}$
398 were seen in Southwest Greenland for the mean 35-year and 2005–2014 periods, respectively.
399 The minimum values of $4.4 \text{ L s}^{-1} \text{ km}^{-2}$ and $6.2 \text{ L s}^{-1} \text{ km}^{-2}$ for the mean 35-year and 2005–2014
400 periods, respectively, occurred in Northeast Greenland (Table 2). On average for the GrIS, the
401 corresponding specific runoffs were $8.1 \text{ L s}^{-1} \text{ km}^{-2}$ and $11.1 \text{ L s}^{-1} \text{ km}^{-2}$, respectively, which are
402 within the range of previous studies (e.g., Mernild et al. 2008). Specific runoff is a valuable tool
403 for comparing runoff on regional and catchment scales, and it can also be used to quantifying the
404 absolute runoff contributions from increasing runoff and increasing melt area extent. The
405 difference in specific runoff between the two periods indicates that the increase in runoff has
406 increased faster than the increase in melt area extent.

407 Refreezing and retention in the snow and firn packs were defined as rain plus surface
408 melt minus runoff (see Section 2.4). For the GrIS, the 35-year mean refreezing and retention was
409 estimated to be 25 % ($140.1 \pm 35.5 \text{ Gt yr}^{-1}$), and it was 22 % ($158.4 \pm 34.4 \text{ Gt yr}^{-1}$) for 2005–
410 2014 (Table 1). Hence, refreezing and retention provided an important quantitative contribution
411 to the evolution of snow and firn layers, ice densities, snow temperatures (cold content or snow



412 temperatures below freezing), and moisture available for runoff (Liston and Mernild 2012). The
413 SnowModel ERA-I refreezing and retention simulations were within the order of magnitude
414 produced by the single-layer snowpack model used by Hanna et al. (2008), but lower than the 45
415 % simulated by Ettema et al. (2009). On the regional-scale, the 35-year mean refreezing and
416 retention value varied from 13 % in North Greenland to 30 % in both Southeast and Southwest
417 Greenland. For 2005–2014, the values were 12 % for North Greenland and 32 % for Southeast
418 Greenland (Table 1), indicating a clear variability in refreezing and retention between the
419 different regions.

420 In Figure 3a, the time series of GrIS mean annual refreezing and retention shows an
421 increasing trend (significant) and variability ranging from ~ 0.05 m w.e. (1992) to ~ 0.14 m w.e.
422 (2012), with an annual mean value of 0.09 ± 0.02 m w.e. In Figure 3b, the spatial 35-year mean
423 GrIS refreezing and retention is presented together with values from 1992 and 2012, the
424 minimum and maximum years, respectively. The mean spatial distribution highlights minimal
425 refreezing and retention at the GrIS interior, whereas areas with low elevation had values above
426 0.8 m w.e. in southern part of the GrIS. For the minimum year 1992, the pattern was more
427 pronounced with no refreezing and retention in the interior. The maximum year 2012 on the
428 other hand had refreezing and retention at the interior (between 0 and 0.02 m w.e.) (Figure 3b).
429 This was likely due to the extreme GrIS surface melt event throughout July 2012 (e.g., Nghiem
430 et al. 2012; Hanna et al. 2014). When divided into regions and catchments, the 2012 simulated
431 refreezing and retention showed a clear separation between highest values in Southwest
432 Greenland and lowest values in Northeast and East Greenland. Because here, refreezing and
433 retention were estimated as the sum of rain and melt minus the sum of runoff, this SnowModel
434 analysis did not provide a detailed description of the physical mechanisms and conditions



435 (beyond the standard SnowModel snowpack temperature and density evolution) leading to, e.g.,
436 non-linearities in snow and firn meltwater retention (Brown et al. 2012). However, while likely
437 an oversimplification of the natural system, this quantitative estimation of refreezing and
438 retention is an important step forward, and improves our runoff and the associated SMB
439 estimates. A model that does not include refreezing and retention processes in its snow and firn
440 evolution calculations, and the associated impacts on SMB, will introduce additional uncertainty
441 in its calculations of GrIS SMB and its contribution to sea-level change.

442 The GrIS SMB for the 35-year mean was $123.7 \pm 163.2 \text{ Gt yr}^{-1}$, indicating a negative sea-
443 level contribution, and $-42.9 \pm 133.5 \text{ Gt yr}^{-1}$ for 2005–2014, indicating a trend towards a positive
444 sea-level contribution (Table 1). This change in SMB between the two periods was mainly due to
445 an increase in runoff of 155.6 Gt yr^{-1} , where other water balance components showed relatively
446 lesser increases. For the GrIS, the 35-year mean SMB was negative for the northern regions,
447 positive for the southern regions and only positive for the southeastern sector for 2005–2014.
448 Overall, the SMB patterns were highly controlled by the distribution of precipitation and runoff.

449 The linear trends for the different water balance components are shown in Table 1. For
450 the 35-year period, only significant trends occurred for rain, surface melt, runoff, ablation, and
451 SMB (highlighted in bold in Table 1), where all except SMB showed positive trends (note that
452 SMB loss is calculated as negative by convention). In Figure 4, selected GrIS parameters are
453 illustrated, where, for example, SMB showed a negative trend of $-99.2 \text{ Gt decade}^{-1}$ (significant),
454 heading towards a zero balance at the end of the simulation period (Figure 4). For 2005–2014,
455 however, the SMB trend was positive $24.2 \text{ Gt decade}^{-1}$ (insignificant). Similar positive SMB
456 trends have previously been shown in studies by Hanna et al. (2011), Tedesco et al. (2014),
457 Fettweis et al., (2008, 2011, 2013) and Wilton et al. (2016), even though variabilities in mean



458 SMB occur between the different studies. Wilton et al. (2016) estimated the GrIS SMB to be
459 $\sim 100 \text{ Gt yr}^{-1}$ in the late-2000s. Further, for 2005–2014, air temperature, precipitation, surface
460 melt, sublimation and evaporation, and runoff trends were all negative (insignificant) (Figure 4
461 and Table 1).

462

463 4.2 Greenland spatiotemporal runoff distribution and EOF analysis

464 The Greenland 35-year simulated catchment outlet runoff and specific runoff distribution
465 are shown in Figure 5. Each circle represents the volume (individual catchment outlet
466 hydrographs are not shown), including runoff from thousands of glaciers located between the
467 GrIS margin and the surrounding seas. The 35-year mean catchment outlet runoff varied from
468 <0.0001 to $25.7 \times 10^9 \text{ m}^3$ (Figure 5a) and specific runoff from <0.1 to $127.5 \text{ L s}^{-1} \text{ km}^{-2}$ (Figure
469 5b). Catchment runoff variability depends on the regional climate conditions, land-ice area
470 cover, elevation range (including hypsometry) within each catchment, and catchment area. Here
471 the length in runoff season varied from two to three weeks in the north to four to six months in
472 the south. The median annual catchment runoff and specific runoff were $0.025 \times 10^9 \text{ m}^3$ and 9.1
473 $\text{L s}^{-1} \text{ km}^{-2}$, respectively. The median specific runoff value is in agreement with previous studies
474 (e.g., Mernild et al. 2010a). Further, the variance in catchment runoff and specific runoff varied
475 from <0.0001 to $8.3 \times 10^9 \text{ m}^3$ and <0.01 to $19.3 \text{ L s}^{-1} \text{ km}^{-2}$, respectively, with a median variance
476 of $0.006 \times 10^9 \text{ m}^3$ and $2.4 \text{ L s}^{-1} \text{ km}^{-2}$ (Figures 4a and 4b). Regarding the linear trend in annual
477 runoff, both increasing and decreasing trends occurred over the 35 years. In total, 81 % (19 %) of
478 all catchments had increasing (decreasing) runoff trends over the 35 years (all of the decreasing
479 trends were insignificant). For western Greenland catchments, only increasing runoff trends
480 occurred (Figures 4a and 4b). The runoff and specific runoff trends varied among catchments



481 from -0.09 to $5.4 \times 10^9 \text{ m}^3 \text{ decade}^{-1}$ and from -1.3 to $12.9 \text{ L s}^{-1} \text{ km}^{-2} \text{ decade}^{-1}$, respectively, with a
482 median value of $0.001 \times 10^9 \text{ m}^3$ and $0.5 \text{ L s}^{-1} \text{ km}^{-2} \text{ decade}^{-1}$ (Figures 4a and 4b).

483 The EOF analysis of runoff returned three axes that captured 25, 17 and 12 % of the
484 variation in runoff from the simulated SnowModel ERA-I annual catchment runoff (Figure 6).
485 Following several significance tests, only EOF1 captured significant variation. In Figure 6, the
486 temporal pattern in EOF1, with a 5-year running mean, reveals a pattern of positive running
487 mean values for the first two decades of the simulation period (1979–1999), and negative values
488 hereafter (2000–2014). When EOF1 is positive, Greenland runoff is relatively low and vice versa
489 (Figure 7). Overall, this indicates a positive temporal trend in runoff; as EOF1 goes down, runoff
490 goes up. While not significant based on EOF test metrics, EOF2 and EOF3 patterns are less
491 pronounced and in anti-phase to each other (Figure 6).

492 The temporal cycle of EOF patterns has associated spatial elements, derived from the
493 eigenvectors (Figure 8). The eigenvectors in Figure 8 reveal the spatial pattern as a correlation
494 between temporal trends captured by the EOFs and each individual Greenland catchment. These
495 data indicate that the temporal trend of increasing runoff captured in EOF1 is shared by nearly all
496 catchments in Greenland. Because decreasing EOF1 values indicate increasing runoff, a negative
497 correlation with EOF1 in space indicates increasing runoff. Catchment numbers greater than
498 #2500 (Figure 8) are located in Southeast Greenland and are in contrast to this. These catchments
499 experience a distinct out-of-phase pattern of runoff compared to the overall Greenland conditions
500 for the last 35 years.

501 This difference between Southeast Greenland and the rest of Greenland supports previous
502 findings (e.g., Lenaerts et al. 2015) proposing that variabilities in runoff are not only influenced
503 by melt conditions, but also by precipitation patterns (primarily the end-of-winter snow



504 accumulation), where high precipitation equals low runoff conditions such as in Southeast
505 Greenland. Furthermore, patterns were also detected to be associated to EOF2 and EOF3
506 (Figures 8b and 8c). These EOF2 and EOF3 patterns differed from EOF1, and they were
507 associated with a different geographic breakdown, where both positive and negative correlations
508 were seen for all regions. The physical mechanism behind these distributions is not clear.

509 There were strong correlations between the EOF1 and regional climate patterns expressed
510 by the AMO and NAO (Figure 9). We found a negative correlation between EOF1 and AMO (r
511 = 0.68; significant, $p < 0.01$), suggesting that stronger AMO is associated with lower EOF1 values
512 which are indicative of higher runoff (Figure 9a). In contrast, we found a positive correlation
513 between EOF1 and NAO ($r = 0.40$; significant, $p < 0.01$), suggesting that stronger NAO values
514 are associated with higher EOF1 values which are indicative of lower runoff (Figure 9b).
515 Additional insight into the time frame over which these correlations arises is seen in Figure 9.
516 For AMO, the lags are centered near zero, suggesting an immediate, real time correlation
517 between AMO and runoff. In contrast, the strongest lag in the NAO-EOF1 relationships is at -2,
518 suggesting a short delay in effects. Lags of 0 and -2 are not large, indicating that overall, large-
519 scale natural variability in AMO and NAO are closely associated in time to catchment runoff
520 variations in Greenland.

521 Mernild et al. (2011) emphasized that trends in AMO (smoothed) was analogous to trends
522 in GrIS melt extent, where increasing AMO equaled increasing melt extent, and vice versa.
523 Further, Chylek et al. (2010) showed that the Arctic detrended temperatures were highly
524 correlated with AMO. However, this issue requires further investigation to establish the details
525 of, and the mechanisms behind, the interrelationships.

526



527 5. Conclusions

528 Greenland catchment outlet runoff is rarely observed and studied, although quantification
529 of runoff from Greenland is crucial for our understanding of the link between a changing climate
530 and changes in the cryosphere, hydrosphere, and atmosphere. We have reconstructed the impact
531 of changes in climate conditions on hydrological processes at the surface of the GrIS for the 35-
532 year period 1979–2014. We have also simulated the Greenland spatiotemporal distribution of
533 refreezing and retention, and freshwater runoff to surrounding seas by merging SnowModel (a
534 spatially distributed meteorological, full surface energy balance, snow and ice evolution model)
535 with HydroFlow (a linear-reservoir run-off routing model) forced by ERA-I atmospheric forcing
536 data. Before simulating the individual catchment runoff to downstream areas, the catchment
537 divides and flow networks were estimated, yielding a total of 3,272 catchments in Greenland.

538 For the GrIS, the simulated spatial distribution and time series of surface hydrological
539 processes were in accordance with previous studies, although precipitation and SMB were in the
540 lower range of these studies. Overall, Greenland has warmed and the runoff from Greenland has
541 increased in magnitude. Specifically, 81 % of the catchments showed increasing runoff trends
542 over the simulation period, with relatively high and low mean catchment runoff from the
543 southwestern and northern parts of Greenland, respectively. This indicates distinct regional-scale
544 runoff variability in Greenland. Runoff variability with near zero lag time suggests a real-time
545 covariation between the pattern in EOF1 and changes in AMO and NAO. This indicates that
546 large-scale natural variability in AMO and NAO is closely related to catchment runoff variations
547 in Greenland. The physical mechanism behind this phenomenon is unclear, unless it is a response
548 to “long-term” cycles in AMO and NAO.



549 The simulated runoff can be used as boundary conditions in ocean models to understand
550 hydrologic links between terrestrial and marine environments in the Arctic. Changes and
551 variability in runoff from Greenland are expected to play an essential role in the hydrographic
552 and circulation conditions in fjords and the surrounding ocean under a changing climate.

553

554 **Acknowledgements**

555 We thank the Japan Society for the Promotion of Science (JSPS) for financial support under
556 project number S17096, and the Western Norway University of Applied Sciences (HVL) for
557 travel funds. All model data requests should be addressed to the first author. The authors have no
558 conflict of interest.

559

560

561

562

563

564

565

566

567

568

569

570

571

572

573

574

575



576 **References**

- 577 AMAP, 2017. Snow, Water, Ice and Permafrost. Summary for Policy-makers. Arctic Monitoring
578 and Assessment Programme (AMAP), Oslo, Norway, 20 pp.
579
- 580 Bales, R. C., Guo, Q., Shen, D., McConnell, J. R., Du, G., Burkhart, J. F., Spikes, V. B., Hanna,
581 E., and Cappelen, J. 2009. Annual accumulation for Greenland updated using ice core data
582 developed during 2000–2006 and analysis, of daily coastal meteorological data. *J. Geophys.*
583 *Res.*, 114, D06116, doi:10.1029/2008JD011208.
584
- 585 Bamber, J., van den Broeke, M., Ettema, J., Lenaerts, J., and Rignot, E., 2012. Recent large
586 increases in freshwater fluxes from Greenland into the North Atlantic. *Geophys. Res. Letts.*, 39,
587 L19501, doi:10.1029/2012GL052552.
588
- 589 Banwell, A., Hewitt, I., Willis, I., and Arnold, N. 2016. Moulin density controls drainage
590 development beneath the Greenland ice sheet. *J. Geophys. Res. Earth Surf.*, 121, 2248–2269.
591
- 592 Bartholomew, I., Nienow, P., Mair, D., Hubbard, A., King, M. A., and Sole, A. 2010. Seasonal
593 evolution of subglacial drainage and acceleration in a Greenland outlet glacier. *Nat. Geosci.*,
594 3(6), 408–411.
595
- 596 Bartholomew, I., Nienow, P., Sole, A., Mair, D., Cowton, T., and King, M. 2012. Short-term
597 variability in Greenland ice sheet motion forces by time-varying meltwater drainage:
598 Implications for the relationship between subglacial drainage system behavior and ice velocity. *J.*
599 *Geophys. Res.*, 117, F03002, doi:10.1029/2011JF002220.
600
- 601 Beamer, J. P., Hill, D. F., Arendt, A., and Liston, G. E. 2016. High-resolution modeling of
602 coastal freshwater discharge and glacier mass balance in the Gulf of Alaska watershed. *Water*
603 *Resour. Res.*, 52, 3888–3909, doi:10.1002/2015WR018457.
604
- 605 Bliss, A., Hock, R., and Radić, V. 2014. Global response of glacier runoff to twenty-first century
606 climate change, *J. Geophys. Res. Earth Surf.*, 119, doi:10.1002/2013JF002931.



607
608 Box, J. E. 2013. Greenland ice sheet mass balance reconstruction, Part II: Surface mass balance
609 (1840–2010). *Journal of Climate*, 26, 6974–6989, doi:10.1175/JCLI-D-12-00518.1.
610
611 Box, J. E., Cappelen, J., Chen, C., Decker, D., Fettweis, X., Mote, T., Tedesco, M., van de Wal,
612 R. S. W., and Wahr, J. 2012. Greenland Ice Sheet. In Jeffries, M. O., Richter-Menge, J. A., and
613 Overland, J. E. (Eds). *Arctic Report Card 2012*, <http://www.arctic.noaa.gov/reportcard>.
614
615 Brown, J., Bradford, J., Harper, J., Pfeffer, W. T., Humphrey, N., and Mosley-Thompson, E.,
616 2012. Georadar-derived estimates of firn density in the percolation zone, western Greenland ice
617 sheet. *Journal of Geophysical Research*, 117, F01011, doi:10.1029/2011JF002089.
618
619 Carrivick, J. L., and Quincey, D. J., 2014. Progressive increase in number and volume of ice-
620 marginal lakes on the western margin of the Greenland Ice Sheet. *Global and Planetary Change*,
621 116, 156-163, doi:10.1016/j.gloplacha.2014.02.009.
622
623 Chen, X., Zhang, X., Church, J. A., Watson, C. S., King, M. A., Monselesan, D., Legresy, B.,
624 and Harig C. 2017. The increasing rate of global mean sea-level rise during 1993–2014. *Nature*
625 *Climate Change*, doi:10.1038/nclimate3325.
626
627 Chu, W., Creyts, T., and Bell, R. E., 2016. Rerouting of subglacial water flow between
628 neighboring glaciers in West Greenland. *J. Geophys. Res. Earth Surf.*, 121, 925–938.
629
630 Church, J. A., Clark, P. U., Cazenave, A., Gregory, J. M., Jevrejeva, S., Levermann, A.,
631 Merrifield, M. A., Milne, G. A., Nerem, R. S., Nunn, P. D., Payne, A. J., Pfeffer, W. T.,
632 Stammer, D., and Unnikrishnan, A. S. 2013. Sea Level Change. In: *Climate Change 2013: The*
633 *Physical Science Basis. Contribution of Working Group I to the Fifth Assessment Report of the*
634 *Intergovernmental Panel on Climate Change* [Stocker, T.F., Qin, D., Plattner, G.-K., Tignor, M.,
635 Allen, S.K., Boschung, J., Nauels, A., Xia, Y., Bex, V. and, Midgley, P.M. (eds.)]. Cambridge
636 University Press, Cambridge, United Kingdom and New York, NY, USA.
637



- 638 Chylek, P., C.K. Folland, G. Lesins and M.K. Dubey. 2010. Twentieth century bipolar seesaw of
639 the Arctic and Antarctic surface air temperatures. *Geophys. Res. Lett.*, 37(8), L08703,
640 doi:10.1029/2010GL042793.
641
- 642 Cuffey, K. M. and Paterson, W. S. B. 2010. *The Physics of Glaciers*. Fourth Edition. Elsevier,
643 pp. 693.
644
- 645 Cullather R. I., Nowicki, S. M. J., Zhao, B., and Koenig, L. S. 2016. A Characterization of
646 Greenland Ice Sheet Surface Melt and Runoff in Contemporary Reanalyses and a Regional
647 Climate Model. *Front. Earth Sci.*, 4(10), doi:10.3389/feart.2016.00010.
648
- 649 Dee, D. P., Uppala, S. M., Simmons, A. J., Berrisford, P., Poli, P., Kobayashi, S., Andrae, U.,
650 Balsameda, M. A., Balsamo, G., Bauer, P., Bechtold, P., Beljaars, A. C. M., van de Berg, L.,
651 Bidlot, J., Bormann, N., Delsol, C., Dragani, R., Fuentes, M., Geer, A. J., Haimberger, L., Healy,
652 S. B., Hersbach, H., Holm, E. V., Isaksen, L., Kållberg, P., Kohler, M., Matricardi, M., McNally,
653 A. P., Monge-Sanz, B. M., Morcrette, J.-J., Park, B.-K., Peubey, C., de Rosnay, P., Tavolato, C.,
654 Thepaut, J.-N., Vitart, F. 2011. The ERA-Interim reanalysis: configuration and performance of
655 the data assimilation system. *Q. J. R. Meteorol. Soc.*, 137, 553–597, doi:10.1002/qj.828.
656
- 657 Dickson, R. R., Osborn, T. J., Hurrell, J. W., Meincke, J., Blindheim, J., Adlandsvik, B., Vinje,
658 T., Alekseev, G., and Maslowski, W. 2000. The Arctic Ocean response to the North Atlantic
659 Oscillation. *Journal of Climate*, 13, 2671–2696.
660
- 661 Enderlin, E. M., Howat, I. M., Jeong, S., Hoh, M.-J., van Angelen, J. H., and van den Broeke, M.
662 R. 2014. An improved mass budget for the Greenland ice sheet. *Geophysical Research Letters*,
663 41(3), 866–872.
664
- 665 Ettema, J., van den Broeke, M. R., van Meijgaard, E., van den Berg, W. J., Bamber, J. L., Box, J.
666 E., and Bales, R. C. 2009. Higher surface mass balance of the Greenland ice sheet revealed by
667 high-resolution climate modeling. *Geophysical Research Letters*, 36, L12501.
668



- 669 Everett, A., Murray, T., Selmes, N., Rutt, I. C., Luckman, A., James, T. D., Clason, S., O'Leary,
670 M., Karunarathna, H., Moloney, V., and Reeve, D. E. 2016. Annual down-glacier drainage of
671 lakes and water-filled crevasses at Helheim Glacier, southeast Greenland. *J. Geophys. Res. Earth*
672 *Surf.*, 121, 1819–1833.
673
- 674 Fettweis, X., Box, J. E., Agosta, C., Amory, C., Kittel, C., Lang, C., van As, D., Machguth, H.,
675 and Gallée, H., 2017. Reconstructions of the 1900–2015 Greenland ice sheet surface mass
676 balance using the regional climate MAR model. *The Cryosphere*, 11, 1015–1033, doi:10.5194/tc-
677 11-1015-2017.
678
- 679 Fettweis, X., Franco, B., Tedesco, M., van Angelen, J. H., Lenaerts, J. T. M., van den Broeke, M.
680 R., and Gallée, H., 2013. Estimating the Greenland ice sheet surface mass balance contribution to
681 future sea level rise using the regional atmospheric climate model MAR. *The Cryosphere*, 7, 709
682 469–489.
683
- 684 Fettweis, X., Hanna, E., Gallée, H., Huybrechts, P., and Erpicum, M. 2008. Estimation of the
685 Greenland ice sheet surface mass balance for the 20th and 21st centuries, *The Cryosphere*, 2,
686 117–129, doi:10.5194/tc-2-117-2008.
687
- 688 Fettweis, X., Tedesco, M., van den Broeke, M., and Ettema, J., 2011. Melting trends over the
689 Greenland ice sheet (1958–2009) from spaceborne microwave data and regional climate models.
690 *The Cryosphere*, 5, 359–375.
691
- 692 Goodison, B. E., Sevruk, B., and Klemm, S. 1989. WMO solid precipitation measurement
693 intercomparison: objectives, methodology, analysis. IAHS publication, 179, 57–64.
694
- 695 Hanna, E., Fettweis, X., Mernild, S. H., Cappelen, J., Ribergaard, M., Shuman, C., Steffen, K.,
696 Wood, L., and Mote, T. 2014. Atmospheric and oceanic climate forcing of the exceptional
697 Greenland Ice Sheet surface melt in summer 2012. *International Journal of Climatology*, 34,
698 1022–1037.
699



- 700 Hanna, E., Huybrechts, P., Cappelen, J., Steffen, K., Bales, R., Burgess, E., McConnell, J.,
701 Steffensen, J. P., Van den Broeke, M., Wake, L., Bigg, B., Griffiths, M., and Savas, D. 2011.
702 Greenland Ice Sheet surface mass balance 1870 to 2010 based on Twentieth Century Reanalysis,
703 and links with global climate forcing, *Journal of Geophysical Research*, 116, D24121,
704 doi:10.1029/2011JD016387.
705
- 706 Hanna, E., Huybrechts, P., Steffen, K., Cappelen, J., Huff, R., Shuman, C., Irvine-Fynn, T.,
707 Wise, S., and Griffiths, M. 2008. Increased runoff from melt from the Greenland ice sheet: A
708 response to global warming. *Journal of Climate*, 21, 331–341.
709
- 710 Hanna, E., McConnell, J., Das, S., Cappelen, J., and Stephens, A. 2006. Observed and modelled
711 Greenland Ice Sheet snow accumulation, 1958–2003, and links with regional climate forcing.
712 *Journal of Climate*, 19(3), 344–358, doi:10.1175/JCLI3615.1.
713
- 714 Hanna, E., Navarro, F. J., Pattyn, F., Domingues, C., Fettweis, X., Ivins, E., Nicholls, R. J., Ritz,
715 C., Smith, B., Tulaczyk, S., Whitehouse, P., and Zwally, J. 2013. Ice-sheet mass balance and
716 climate change. *Nature*, 498, 51–59.
717
- 718 Hanna, E., Mernild, S. H., Cappelen, J., and Steffen, K. 2012. Recent warming in Greenland in a
719 long-term instrumental (1881–2012) climatic context. Part 1: Evaluation of surface air
720 temperature records. *Environmental Research Letters*, 7, 045404, doi:10.1088/1748-
721 9326/7/4/045404.
722
- 723 Haper, J., Humphrey, N., Pfeffer, W. T., Brown, J. and Fettweis, X. 2012. Greenland ice-sheet
724 contribution to sea-level rise buffered by meltwater storage in firn. *Nature*, 22117–22124.
725
- 726 Hasholt, B., Mikkelsen, A. B., Nielsen, H. M., and Larsen, M. A. D. 2013. Observations of
727 Runoff and Sediment and Dissolved Loads from the Greenland Ice Sheet at Kangerlussuaq, West
728 Greenland, 2007 to 2010. *Zeitschrift für Geomorphologie*, 57(2), 3–27, doi:10.1127/0372-
729 8854/2012/S-00121.
730



- 731 Hewitt, I. 2013. Seasonal changes in ice sheet motion due to melt water lubrication. *Earth Plant.*
732 *Sci. Lett.*, 371–372, 16–25.
733
- 734 Hiemstra, C. A., Liston, G. E., and Reiners, W. A. 2006. Observing, modelling, and validating
735 snow redistribution by wind in a Wyoming upper treeline landscape. *Ecol. Model.* 197, 35–51,
736 doi: 10.1016/j.ecolmodel.2006.03.005.
737
- 738 Howat, I. M., De la Peña, S., Van Angelen, J. H., Lenaerts, J. T. M., and Van den Broeke, M. R.
739 2013. Expansion of meltwater lakes on the Greenland Ice Sheet. *The Cryosphere*, 7, 201–204.
740 doi:10.5194/tc-7-201-2013.
741
- 742 Hurrell, J. W. 1995. Decadal trends in the North Atlantic Oscillation: regional temperatures and
743 precipitation. *Science*, 269, 676–679. doi:10.1126/science.269.5224.676.
744
- 745 Hurrell, J. W. and van Loon, H. 1997. Decadal variations in climate associated with the North
746 Atlantic oscillation, *Climate Change*, 36, 301–326.
747
- 748 Kaplan, A., Cane, M. A., Kushnir, Y. and Clement, A. C. 1998. Analyses of global sea surface
749 temperatures 1856–1991. *Journal of Geophysical Research*, 103, 18575–18589.
750
- 751 Kobayashi, S., Ota, Y., Harada, Y., Ebata, A., Moriya, M., Onoda, H., Onogi, K., Kamahori, H.,
752 Kobayashi, C., Endo, H., Miyaoka, K., and Takahashi, K. 2015. The JRA-55 Reanalysis:
753 General Specifications and Basic Characteristics, *J. Meteorol. Soc. Jpn.*, 93, 5–48,
754 doi:10.2151/jmsj.2015-001.
755
- 756 Kohler, T. J., Zarsky, J. D., Yde, J. C., Lamarche-Gagnon, G., Hawkings, J. R., Tedstone, A. J.,
757 Wadham, J. L., Box, J. E., Beaton, A., and Stibal, M., 2017. Carbon dating reveals seasonal
758 shifts in the source of sediments exported from the Greenland Ice Sheet. *Geophys. Res. Lett.*,
759 44(12), 6209–6217.
760



- 761 Koziol, C., Arnold, N., Pope, A., and Colgan, W., 2017. Quantifying supraglacial meltwater
762 pathways in the Paakitsoq region, West Greenland. *J. Glaciol.*, 63(239), 464–476.
763
- 764 Langen, P. L., Mottram, R. H., Christensen, J. H., Boberg, F., Rodehacke, C. B., Stendel, M., van
765 As, D., Ahlstrøm, A. P., Mortensen, J., Rysgaard, S., Petersen, D., Svendsen, K. H.,
766 Algeirsdottir, G. A., and Cappelen, J. 2015. Quantifying Energy and Mass Fluxes Controlling
767 Godthåbsfjord Freshwater Input in a 5-km Simulation (1991–2012). *Journal of Climate*, 28,
768 3694–3713, doi:10.1175/JCLI-D-14-00271.1.
769
- 770 Lenaerts, J. T. M., Le Bars, D., van Kampenhout, L., Vizcaino, M., Enderlin, E. M., and van den
771 Broeke, M. R. 2015. Representing Greenland ice sheet freshwater fluxes in climate models.
772 *Geophys. Res. Lett.*, 42, 6373–6381, doi:10.1002/2015GL064738.
773
- 774 Levinsen, J. F., Forsberg, R., Sørensen, L. S., and Khan, S. A. 2015. Essential Climate Variables
775 for the Ice Sheets from Space and Airborne measurements. Danmarks Tekniske Universitet
776 (DTU) PhD Thesis, Kgs. Lyngby, pp. 1–232.
777
- 778 Lewis, S. M., and Smith, L. C. 2009. Hydrological drainage of the Greenland ice sheet. *Hydrol.*
779 *Processes*, 23, 2004–2011, doi:10.1002/hyp.7343.
780
- 781 Liston, G. E. 1995. Local advection of momentum, heat, and moisture during the melt of patchy
782 snow covers. *J. Appl. Meteorol.*, 34, 1705–1715, doi:10.1175/1520-0450-34.7.1705.
783
- 784 Liston, G. E. and Elder, K. 2006a. A distributed snow-evolution modeling system (SnowModel).
785 *J. Hydrometeorol.*, 7, 1259–1276, doi:10.1175/JHM548.1.
786
- 787 Liston, G. E. and Elder, K. 2006b. A meteorological distribution system for high-resolution
788 terrestrial modeling (MicroMet). *J. Hydrometeorol.*, 7, 217–234, doi:10.1175/JHM486.1.
789



- 790 Liston, G. E., Haehnel, R. B., Sturm, M., Hiemstra, C. A., Berezovskaya, S., and Tabler, R. D.
791 2007. Simulating complex snow distributions in windy environments using SnowTran-3D. *J.*
792 *Glaciol.*, 53, 241–256.
793
- 794 Liston, G. E. and Hiemstra, C. A. 2011. The changing cryosphere: pan-Arctic snow trends
795 (1979–2009). *J. Clim.*, 24, 5691–5712.
796
- 797 Liston, G. E. and Mernild, S. H. 2012. Greenland freshwater runoff. Part I: a runoff routing
798 model for glaciated and non-glaciated landscapes (HydroFlow). *J. Clim.*, 25(17), 5997–6014.
799
- 800 Liston, G. E. and Sturm, M. 1998. A snow-transport model for complex terrain. *J. Glaciol.*, 44,
801 498–516.
802
- 803 Liston, G. E. and Sturm, M. 2002. Winter precipitation patterns in Arctic Alaska determined from
804 a blowing-snow model and snow depth observations. *J. Hydrometeorol.*, 3, 646–659.
805
- 806 Liston, G. E., Winther, J.-G., Bruland, O., Elvehøy, H., and Sand, K. 1999. Below surface ice
807 melt on the coastal Antarctic ice sheet. *J. Glaciol.*, 45, 273–285.
808
- 809 Machguth, H., MacFerrin, M., van as, D., Box, J., Charalampidis, C., Colgan, W., Fausto, R. S.,
810 Meijer, H. A. J., Mosley-Yhompson, E., and van de Wal, R. S. W. 2016. Greenland meltwater
811 storage in firn limited by near-surface ice formation. *Nature Climate Change*, 6(4), 390–393,
812 doi.org/10.1038/nclimate2899.
813
- 814 Mernild, S. H., B. Hasholt and G. E. Liston 2006b. Water flow through Mittivakkat Glacier,
815 Ammassalik Island, SE Greenland. *Geografisk Tidsskrift-Danish Journal of Geography*, 106(1),
816 25–43.
817
- 818 Mernild, S. H., Hanna, E., McConnell, J. R., Sigl, M., Beckerman, A. P., Yde, J. C., Cappelen, J.,
819 and Steffen, K. 2015. Greenland precipitation trends in a long-term instrumental climate context



- 820 (1890–2012): Evaluation of coastal and ice core records. *International Journal of Climatology*,
821 35, 303–320, doi:10.1002/joc.3986.
822
- 823 Mernild, S. H. and Liston, G. E. 2010. The influence of air temperature inversion on snow melt
824 and glacier surface mass-balance simulations, SW Ammassalik Island, SE Greenland. *Journal of*
825 *Applied Meteorology and Climate*, 49(1), 47–67.
826
- 827 Mernild, S. H. and Liston, G. E. 2012. Greenland freshwater runoff. Part II: distribution and
828 trends, 1960–2010. *J. Clim.*, 25(17), 6015–6035.
829
- 830 Mernild, S. H., Liston, G. E., Hasholt, B., and Knudsen, N. T. 2006a. Snow distribution and melt
831 modeling for Mittivakkat Glacier, Ammassalik Island, SE Greenland. *Journal of*
832 *Hydrometeorology*, 7, 808–824.
833
- 834 Mernild, S. H., and Liston, G. E., and Hiemstra, C. A. 2014. Northern hemisphere glaciers and
835 ice caps surface mass balance and contribution to sea-level rise. *J. Clim.*, 27(15), 6051–6073,
836 doi:10.1175/JCLI-D-13-00669.1.
837
- 838 Mernild, S. H., Liston, G. E., Hiemstra, C. A. and Christensen, J. H. 2010a. Greenland Ice Sheet
839 surface mass-balance modeling in a 131 year perspective 1950–2080. *Journal of*
840 *Hydrometeorology*, 11(1), 3–25, doi.org/10.1175/2009JHM1140.1.
841
- 842 Mernild, S. H., Liston, G. E., Hiemstra, C. A., and Steffen, K. 2008. Surface Melt Area and
843 Water Balance Modeling on the Greenland Ice Sheet 1995–2005. *Journal of Hydrometeorology*,
844 9(6), 1191–1211, doi.org/10.1175/2008JHM957.1.
845
- 846 Mernild, S. H., Liston, G. E., van As, D., Hasholt, B., and Yde, J. C. 2017. High-resolution ice
847 sheet surface mass-balance and spatiotemporal runoff simulations: Kangerlussuaq, West
848 Greenland. Accepted *Arctic, Antarctic, and Alpine Research* (Special Issue, Kangerlussuaq).
849



- 850 Mernild, S. H., Mote, T., and Liston, G. E. 2011. Greenland Ice Sheet surface melt extent and
851 trends, 1960–2010. *Journal of Glaciology*, 57(204), 621–628.
852
- 853 Metcalfe, J. R., Ishida, S., and Goodison, B. E. 1994. A corrected precipitation archive for the
854 Northwest Territories of Canada,
855 http://www.usask.ca/geography/MAGS/Data/Public_Data/precip_corr/pcpncor_e.htm.
856
- 857 Nghiem, S. V., Hall, D. K., Mote, T. L., Tedesco, M., Albert, M. R., Keegann, K., Shuman, C.
858 A., DiGirolamo, N. E., and Neumann, G. 2012. The extreme melt across the Greenland ice sheet
859 in 2012. *Geophysical Research Letters*, 39, L20502.
860
- 861 Nick, F. M., Vieli, A., Howat, I. M., and Joughin, I. R. 2009. Large-scale changes in Greenland
862 outlet glacier dynamics triggered at the terminus. *Nature Geoscience*, 2(2), 110–114,
863 doi:10.1038/ngeo394.
864
- 865 Noël, B., van de Berg, W. L., Lhermitte, S., Wouters, B., Machguth, H., Howat, I., Citterio, M.,
866 Moholdt, G., Lenaerts, J. T. M., and van den Broeke, M. R. 2017. A tipping point in refreezing
867 accelerates mass loss of Greenland’s glaciers and ice caps. *Nature Communications*, 8, 1–8,
868 doi:10.1038/ncomms14730.
869
- 870 Overland, J. E., Francis, J., Hanna, E. and Wang, M. 2012. The recent shift in early summer
871 arctic atmospheric circulation. *Geophysical Research Letters*, 39, L19804.
872
- 873 Preisendorfer, R.W. 1998. *Principal Component Analysis in Meteorology and Oceanography*. In:
874 Mobley, C.D. (Ed.) Elsevier, Amsterdam, p. 452.
875
- 876 Rahmstorf, S., and Coauthors. 2005. Thermohaline circulation hysteresis: A model
877 intercomparison. *Geophys. Res. Lett.*, 32, L23605, doi:10.1029/2005GL023655.
878
- 879 Rasmussen, R., Baker, B., Kochendorfer, J., Meyers, T., Landolt, S., Fischer, A. P., Black, J.,
880 Theriault, J. M., Kucera, p., Gochis, D., Smith, C., Nitu, R., Hall, M., Ikeda, K., and Gutmann,



- 881 E. 2012. How well are we measuring snow? The NOAA/FAA/NCAR Winter Precipitation Test
882 Bed. BAMS, 811–829.
883
- 884 Rignot, E. and Mouginot, J. 2012. Ice flow in Greenland for the International Polar Year 2008–
885 2009. Geophysical Research Letters, 39, L11501, doi:10.1029/2012GL051634.
886
- 887 Rignot, E., Velicogna, I., van den Broeke, M. R., Monaghan, A., and Lenaerts, J. 2011.
888 Acceleration of the contribution of the Greenland and Antarctic ice sheets to sea level rise.
889 Geophysical Research Letters, 38, L05503.
890
- 891 Roberts, M.J. 2005. Jökulhlaups: a reassessment of floodwater flow through glaciers. Rev.
892 Geophys., 43(1), RG1002, doi:10.1029/2003RG000147.
893
- 894 Rogers, A. N., Bromwich, D. H., Sinclair, E. N. and Cullather, R. I., 2001. The atmospheric
895 hydrological cycle over the Arctic basins from reanalysis. Part II: Inter-annual variability.
896 Journal of Climate, 14, 2414–2429.
897
- 898 Selmes, N., Murray, T., and James, T. D. 2011. Fast draining lakes on the Greenland ice sheet.
899 Geophys Res. Lett., 38(15), doi:10.1029/2011GL047872.
900
- 901 Shepherd, A. et al. 2012. A Reconciled Estimate of Ice-Sheet Mass Balance. Science, 338,
902 1183–1189.
903
- 904 Sparnocchia S, Pinardi N, and Demirov E. 2003. Multivariate empirical orthogonal function
905 analysis of the upper thermocline structure of the Mediterranean Sea from observations and
906 model simulations. Ann. Geophys, 21, 167–187.
907
- 908 Sugden, D.E., Clapperton, C. M, and Knight, P. G. 1985. A jökulhlaup near Søndre Strømfjord,
909 West Greenland, and some effects on the ice-sheet margin. Journal of Glaciology, 31(109), 366–
910 368.
911



- 912 Steffen, K. 1995. Surface energy exchange at the equilibrium line on the Greenland ice sheet
913 during onset of melt. *Annals of Glaciology*, 21, 13–18.
914
- 915 Straneo, F., Curry, R. G., Sutherland, D. A., Hamilton, G. S., Cenedese, C., Våge, K., and Sterns,
916 L. A. 2011. Impact of fjord dynamics and glacial runoff on the circulation near Helheim Glacier.
917 *Nat. Geosci.*, 4, 322–327, doi:10.1038/ngeo1109.
918
- 919 Tedesco, M., Willis, I. C., Hoffman, M. J., Banwell, A. F., Alexander, P., and Arnold, N. S.
920 2013. Ice dynamic response to two modes of surface lake drainage on the Greenland ice sheet.
921 *Environ. Res. Lett.*, 8(3), 34007, doi:10.1088/1748-9326/8/3/034007.
922
- 923 Tedesco, M., Box, J. E., Cappelen, J., Fettweis, X., Mote, T., van de Wal, R. S. W., Smeets, C. J.
924 P. P., and Wahr, J. 2014. Greenland Ice Sheet. In Jeffries, M. O., Richter-Menge, J. A., and
925 Overland, J. E. (eds.). *Arctic Report Card 2014*.
926
- 927 Tedesco, M., Box, J. E., Cappelen, J., Fausto, R. S., Fettweis, X., Mote, T., Smeets, C. J. P. P.,
928 van As, D., Velicogna, I., van de Wal, R. S. W. and Wahr, J. 2016. Greenland Ice Sheet. In
929 Richter-Menge, J. A., Overland, J. E., and Mathis, J. T. (eds.). *Arctic Card Report 2016*.
930
- 931 Uppala, S. M., Kållberg, P. W., Simmons, A. J., Andrae, U., Da Costa Bechtold, V., Fiorino, M.,
932 Gibson, J. K., Haseler, J., Hernandez, A., Kelly, G. A., Li, X., Onogi, K., Saarinen, S., Sokka,
933 N., Allan, R. P., Anderson, E., Arpe, K., Balmaseda, M. A., Beljaars, A. C. M., Van De Berg, L.,
934 Bidlot, J., Bormann, N., Caires, S., Chevallier, F., Dethof, A., Dragosavac, M., Fisher, M.,
935 Fuentes, M., Hagemann, S., Hólm, E., Hoskins, B. J., Isaksen, L., Janssen, P. A. E. M., Jenne, R.,
936 McNally, A. P., Mahfouf, J.-F., Morcrette, J.-J., Rayner, N. A., Saunders, R. W., Simon, P., Sterl,
937 A., Trenbreth, K. E., Untch, A., Vasiljevic, D., Viterbo, P., and Woollen, J.: The ERA-40 re-
938 analysis, *Q. J. Roy. Meteor. Soc.*, 131, 2961–3012, doi:10.1256/qj.04.176, 2005.
939
- 940 van Angelen, J. H., Lenaerts, J. T. M., van den Broeke, J. T. M., Fettweis, X., van Meijgaard, E.
941 2013. Rapid loss of firn pore space accelerates 21 century Greenland mass loss. *Geophysical*
942 *Research Letter*, 40, 2109–2113.



943
944 van As., D, Box, J. E., and Fausto, R. S., 2016: Challenges of Quantifying Meltwater Retention
945 in Snow and Firn: An Expert Elicitation. *Frontiers in Earth Science*, 4(101), 1–5.
946
947 van den Broeke, M., Smeets, P., Ettema, J., and Munneke, P. K. 2008a. Surface radiation balance
948 in the ablation zone of the west Greenland ice sheet, *J. Geophys. Res.*, 113, D13105,
949 doi:10.1029/2007/JD009283.
950
951 van den Broeke, M., Smeets, P., Ettema, J., van der Veen, C., van de Wal, R., and Oerlemans, J.
952 2008b. Partitioning of melt energy and meltwater fluxes in the ablation zone of the west
953 Greenland ice sheet, *The Cryosphere*, 2, 179–189, doi:10.5194/tc-2-179-2008.
954
955 van de Wal, R. S. W., Greuell, W., van den Broeke, M. R., Reijmer, C. H., and Oerlemans, J.
956 2005. Surface mass-balance observations and automatic weather station data along a transect
957 near Kangerlussuaq, West Greenland, *Ann. Glaciol.*, 42, 311–316.
958
959 van de Wal, R. S. W., Boot, W., van den Broeke, M., Smeets, C. J. P. P., Reijmer, C. H., Donker,
960 J. J. A., and Oerlemans, J. 2008. Large and rapid melt-induced velocity changes in the ablation
961 zone of the Greenland ice sheet. *Science*, 321, 111–113.
962
963 van der Veen, C. J. 2007. Fracture propagation as a means of rapidly transferring surface
964 meltwater to the base of glaciers. *Geophys. Res. Lett.*, 34, L01501.
965
966 Weijer, W., M. E. Maltrud, M. W. Hecht, H. A. Dijkstra, and M. A. Kliphuis, 2012. Response of
967 the Atlantic Ocean circulation to Greenland Ice Sheet melting in a strongly-eddy ocean
968 model. *Geophys. Res. Lett.*, 39, L09606, doi:10.1029/2012GL051611.
969
970 Wilton, D. J., Jowett, A., Hanna, E., Bigg, G. R., van den Broeke, M. R., Fettweis, X., and
971 Huybrechts, P., 2017. High resolution (1 km) positive degree-day modelling of Greenland ice
972 sheet surface mass balance, 1870-2012 using reanalysis data. *Journal of Glaciology*, 63(237),
973 176–193.



974

975 Yang, D., Ishida, S., Goodison, B. E., and Gunter, T. 1999. Bias correction of daily precipitation
976 measurements for Greenland. *J. Geophys. Res.* 104(D6), 6171–6181,
977 doi:10.1029/1998JD200110.

978

979 Zwally, H. J., Abdalati, W., Herring, T., Larson, K., Saba, J., and Steffen, K. 2002. Surface melt-
980 induced acceleration of Greenland ice-sheet flow. *Science*, 297, 218–222.

981

982

983

984

985

986

987

988

989

990

991

992

993

994

995

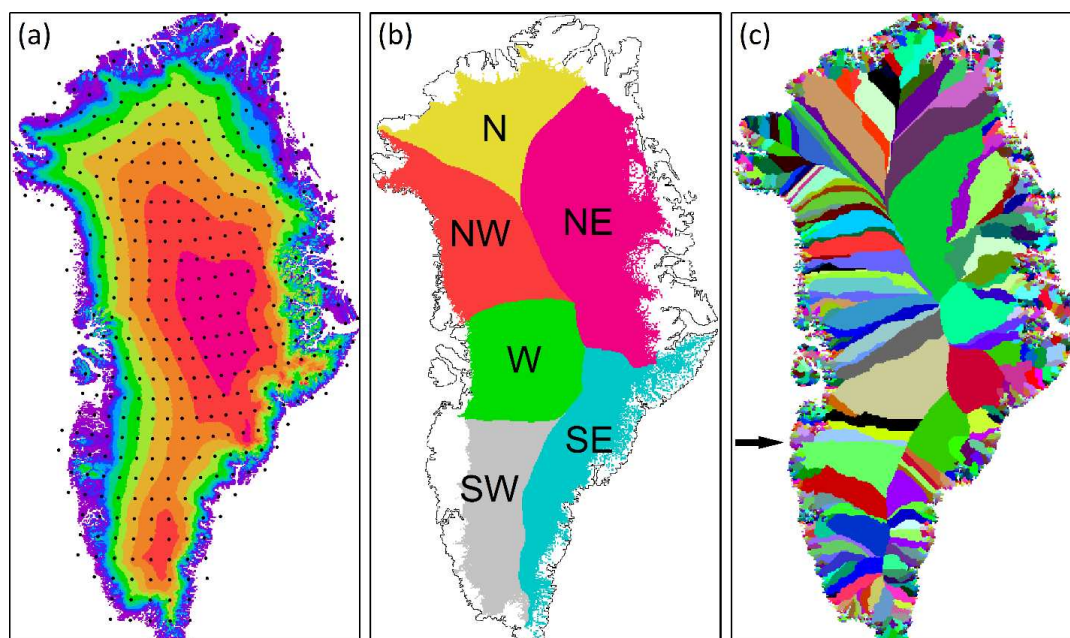
996

997

998

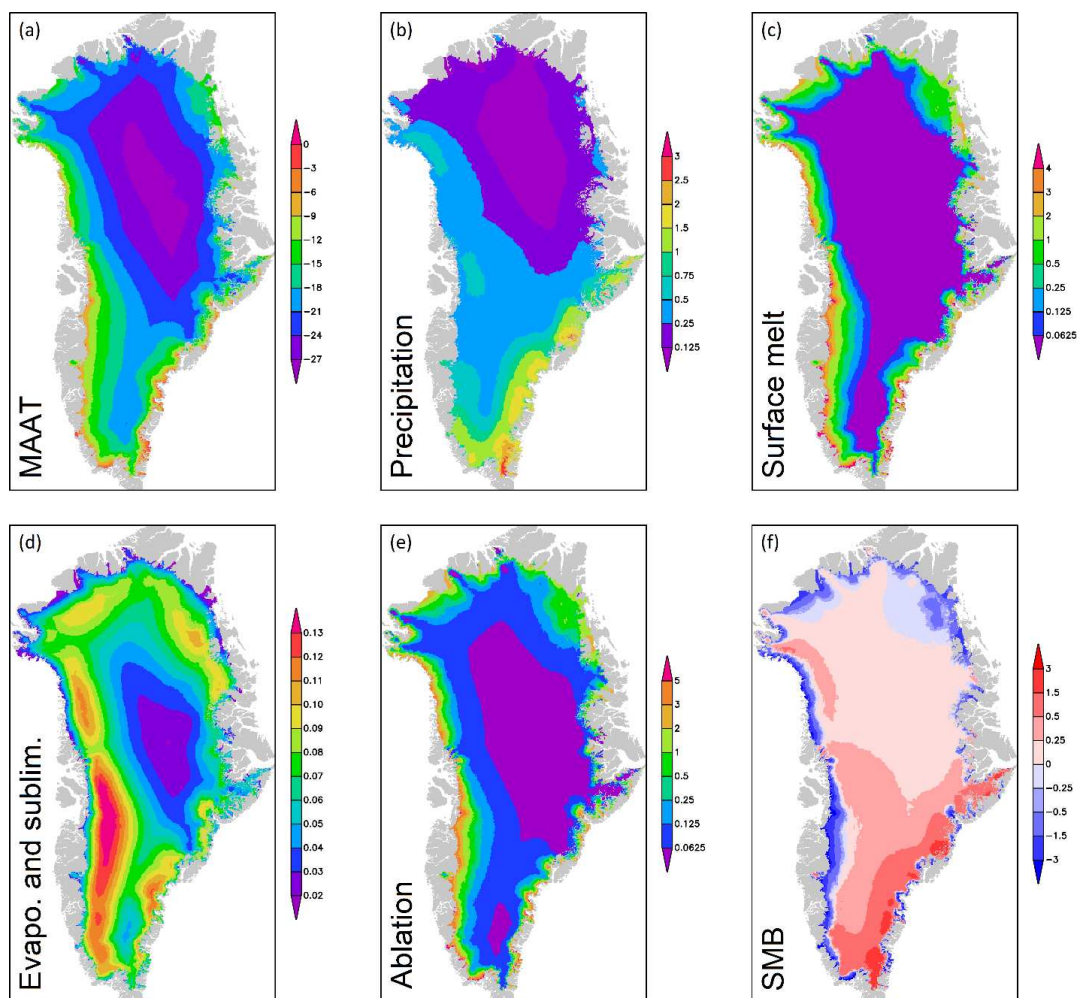
999

1000



1001
1002 **Figure 1:** (a) Greenland simulation domain with topography (500-m contour interval) and
1003 locations of ERA-I atmospheric forcing grid points used in the model simulations (black dots; to
1004 improve clarity only every other grid point was plotted in x and y, i.e., 25 % of the grid points
1005 used are shown); (b) the major regional division of the GrIS following Rignot et al.
1006 (unpublished); and (c) HydroFlow simulated individual Greenland drainage catchments (n =
1007 3,272; represented by multiple colors). The approximate location of the Kangerlussuaq
1008 catchment is shown with a black arrow.

1009
1010
1011
1012
1013



1014

1015 **Figure 2:** SnowModel ERA-I simulated 35-year mean spatial GrIS surface (1979–2014): (a)

1016 MAAT (°C); (b) precipitation (m w.e.); (c) surface melt (snow and ice melt) (m w.e.); (d)

1017 evaporation and sublimation (m w.e.); (e) ablation (m w.e.); and (f) SMB (m w.e.).

1018

1019

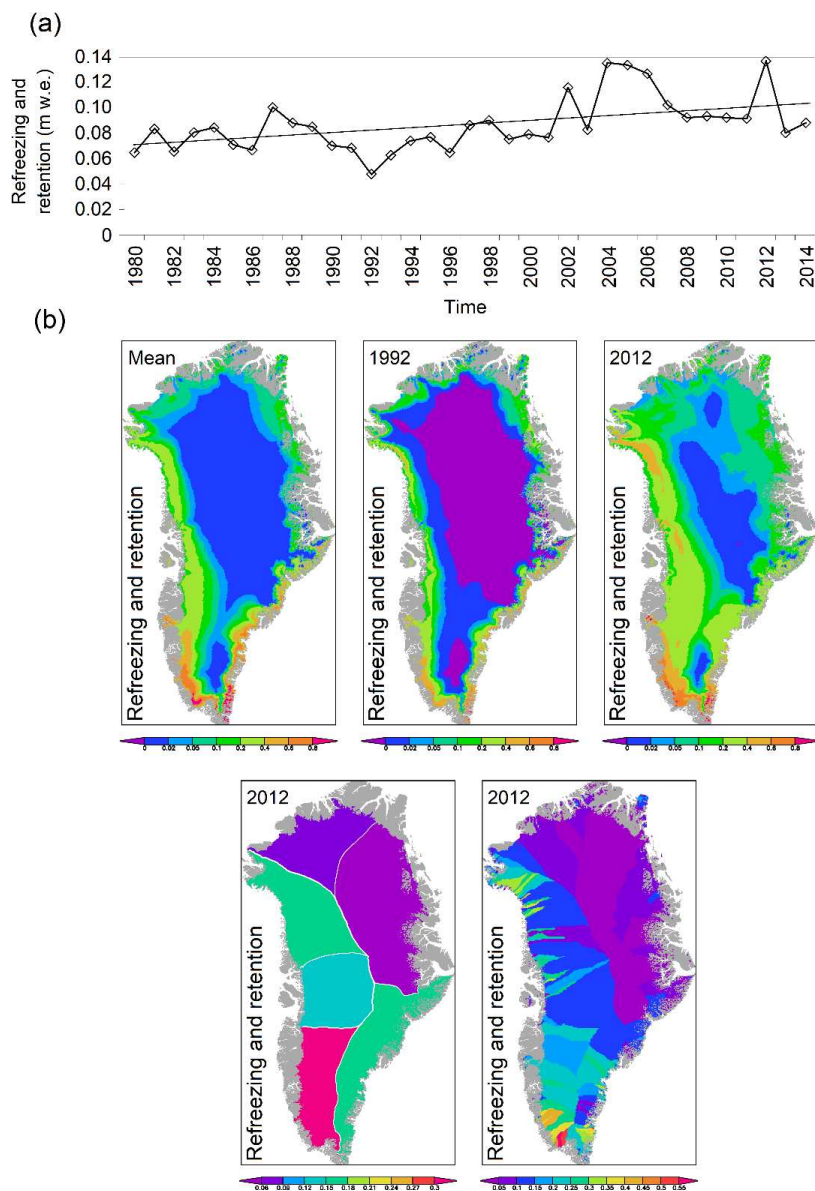
1020

1021

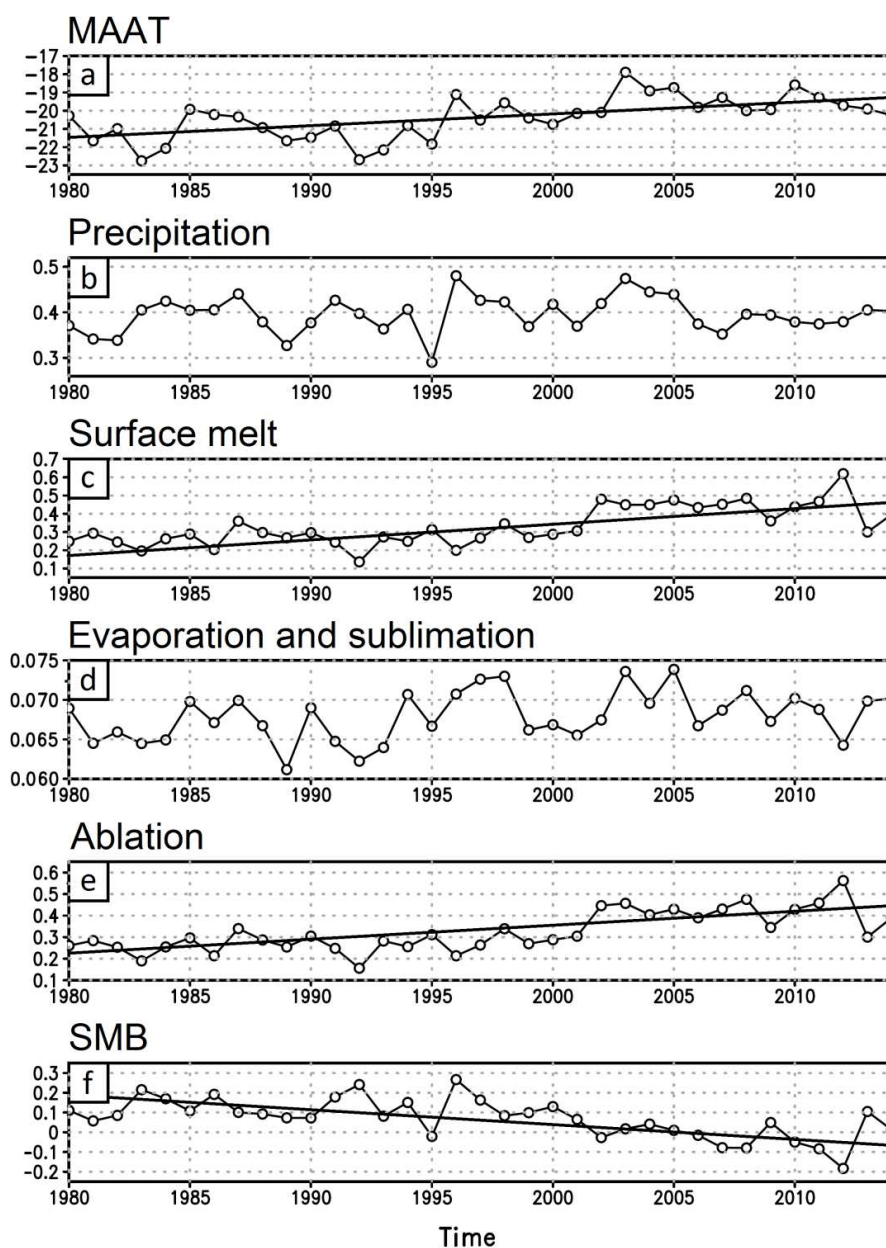
1022

1023

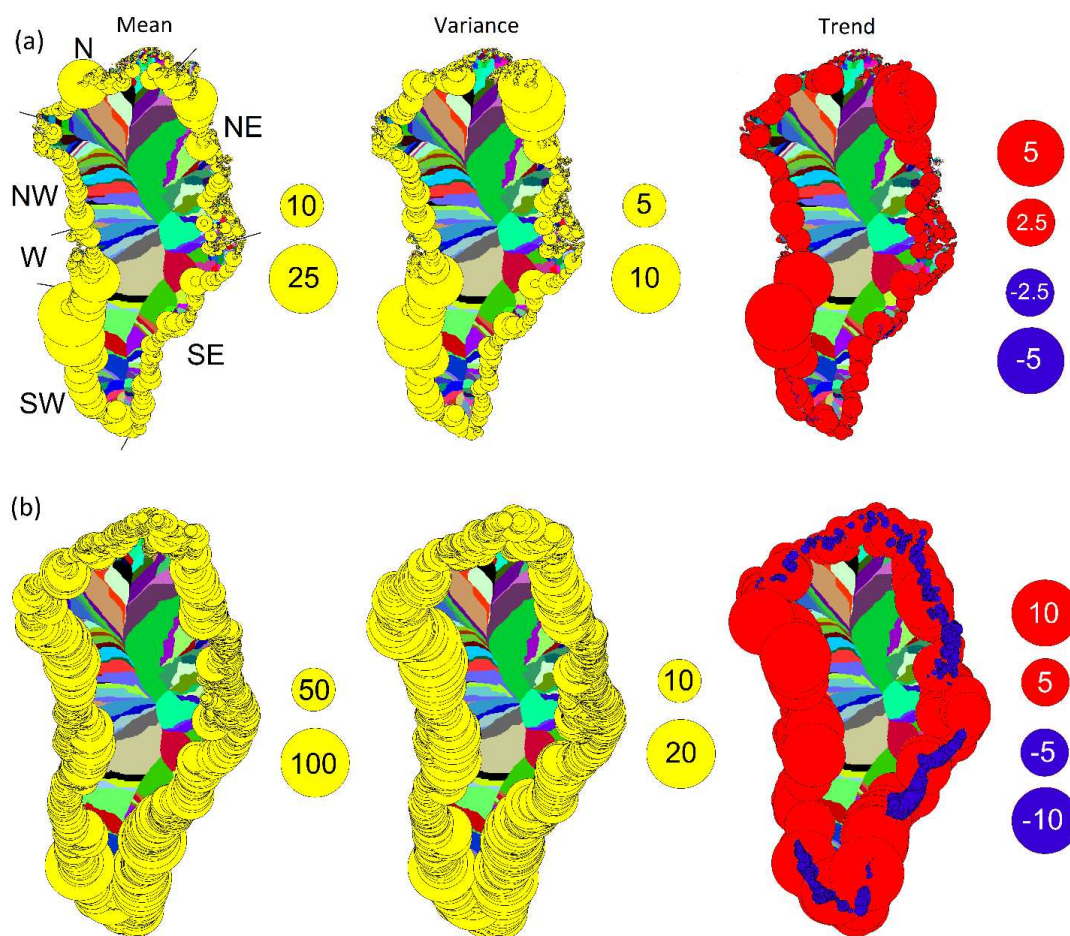
1024



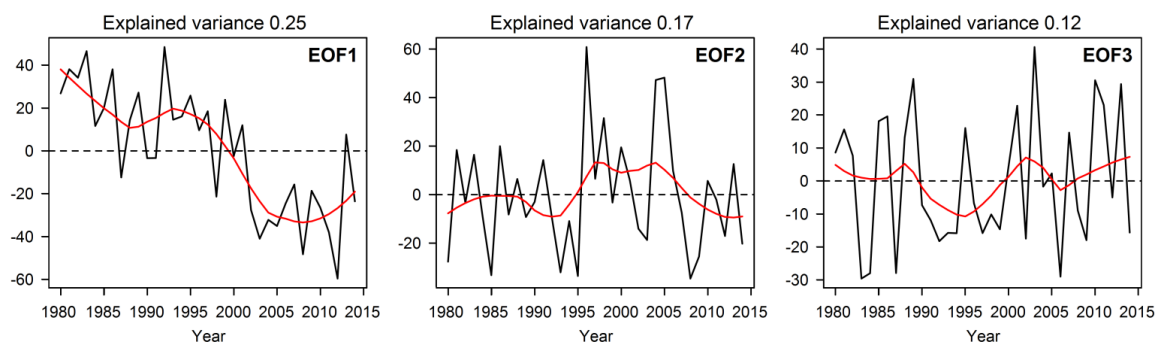
1025
 1026 **Figure 3:** (a) SnowModel ERA-I simulated time series of GrIS mean annual refreezing and
 1027 retention (1979–2014) (m w.e.); and (b) spatial 35-year mean GrIS refreezing and retention and
 1028 annual values (m w.e) for 1992 and 2012 (upper row), together with the 2012-division into
 1029 regions (lower row left) and catchments (lower row right).



1030
1031 **Figure 4:** SnowModel ERA-I simulated time series of GrIS annual mean (1979–2014): (a)
1032 MAAT (°C); (b) precipitation (m w.e.); (c) surface melt (snow and ice melt) (m w.e.); (d)
1033 evaporation and sublimation (m w.e.); (e) ablation (m w.e.); and (f) SMB (m w.e.). Only
1034 significant linear trends are shown.



1035
 1036 **Figure 5:** SnowModel ERA-I simulated 35-year spatial Greenland catchment runoff (1979–
 1037 2014): (a) mean runoff ($\times 10^9 \text{ m}^3$) (the locations of the major regions SW, W, NW, etc., are
 1038 illustrated), runoff variance (here illustrated as one standard deviation; $\times 10^9 \text{ m}^3$), and decadal
 1039 runoff trends (linear; $\times 10^9 \text{ m}^3 \text{ decade}^{-1}$) (catchments with increasing runoff trends are shown
 1040 with red and decreasing trends with blue colors); and (b) mean specific runoff ($\text{L s}^{-1} \text{ km}^{-2}$),
 1041 specific runoff variance ($\text{L s}^{-1} \text{ km}^{-2}$), and specific runoff trends (linear; $\text{L s}^{-1} \text{ km}^{-2} \text{ decade}^{-1}$).
 1042



1043

1044 **Figure 6:** SnowModel ERA-I simulated runoff time series (1979–2014) of the empirical
1045 orthogonal functions (black curve) and 5-year running mean smoothing line (red curve) of EOF1,
1046 EOF2, and EOF3. The explained variance is shown for each EOF, where only EOF1 is
1047 significant.

1048

1049

1050

1051

1052

1053

1054

1055

1056

1057

1058

1059

1060

1061

1062

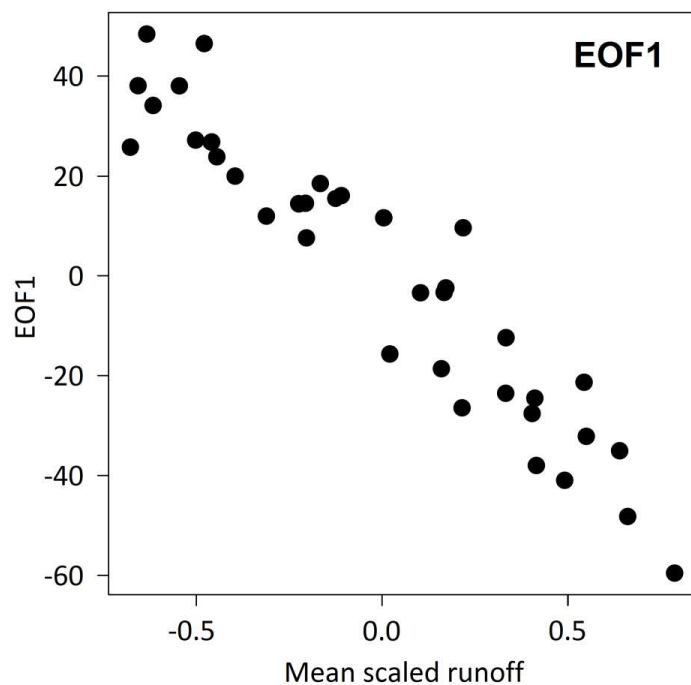
1063

1064

1065

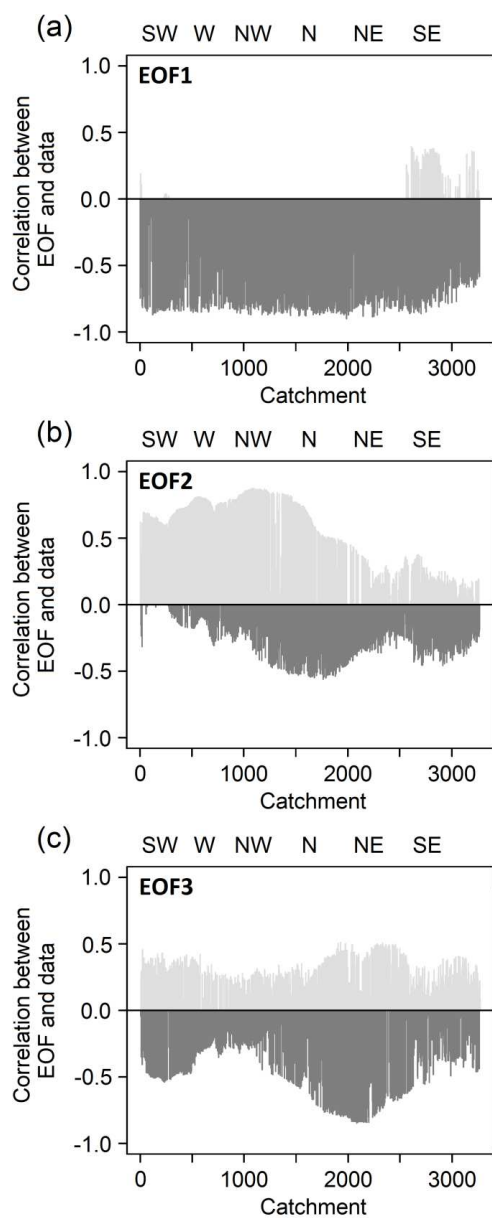
1066

1067



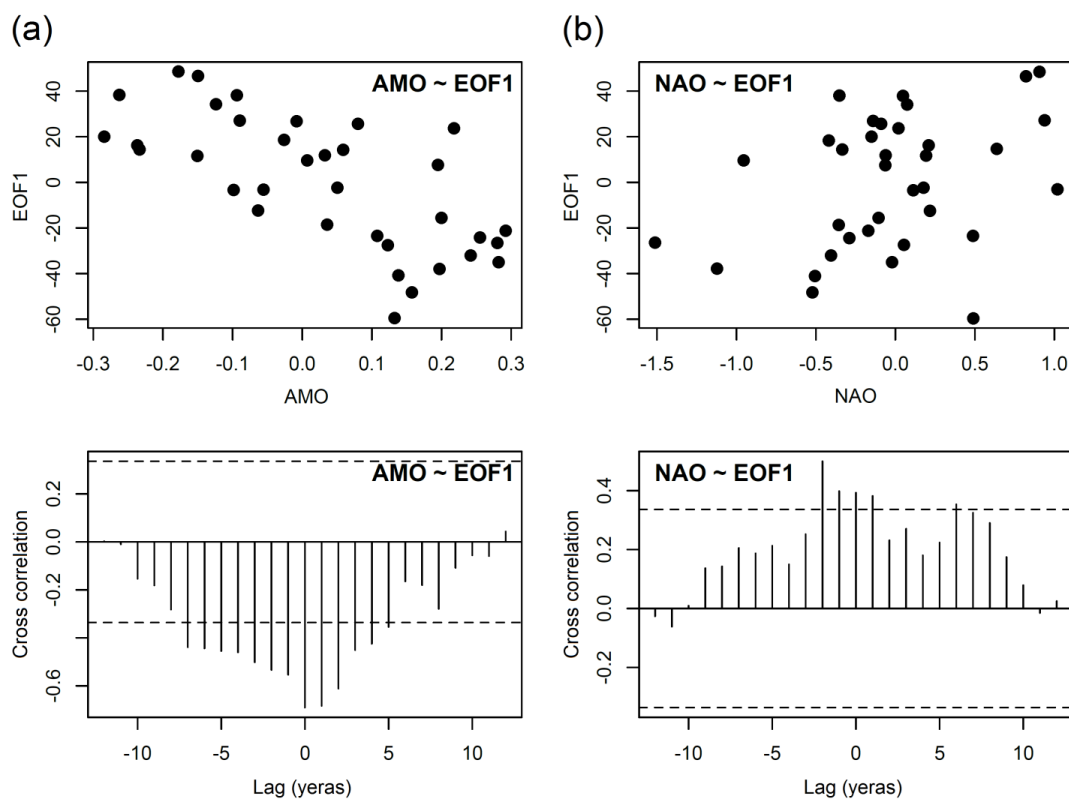
1068

1069 **Figure 7:** EOF1 cross correlation relationships with mean annual scaled runoff from Greenland.



1070

1071 **Figure 8:** Eigenvector correlation values for each simulated catchment (1 to 3,272) for: (a)
1072 EOF1; (b) EOF2; and (c) EOF3. From left to right on the lower x-axis the catchments follows the
1073 clockwise path from the southern tip of Greenland (Southwest Greenland, Catchment 1) to the
1074 northern part (N section) and back to the southern tip (Southeast Greenland, Catchment 3,272).
1075 The location of the major regions: SW, W, NW, etc., are shown on the upper x-axis.



1076

1077 **Figure 9:** EOF1 cross correlation relationships between simulated Greenland runoff: (a) AMO
1078 and (b) NAO. The horizontal dashed lines on each of the column charts indicate the significance
1079 (95% confidence).

1080

1081

1082

1083

1084

1085

1086

1087



1088 **Table 1:** Regional breakdown of GrIS surface mean annual conditions (units are in Gt) and
 1089 trends (linear; Gt decade⁻¹): precipitation (P) (including rain and snow), surface melt, evaporation
 1090 (E) and sublimation (Su), runoff (R), ablation, refreezing and retention, and surface mass-balance
 1091 (SMB) for GrIS and for each of the six regions both from 1979–2014 (35 years) and 2005–2014
 1092 (10 years). Specifically for rain the %-value of total precipitation is shown. Trends are shown in
 1093 paragraphs for the GrIS column. Significant trends ($p < 0.05$) are highlighted in bold.

	N (229,075 km ²)	NE (454,900 km ²)	SE (250,425 km ²)	SW (213,550 km ²)	W (231,150 km ²)	NW (267,075 km ²)	GrIS (1,646,175 km ²)
1979–2014							
P	31.1 ± 5.4	68.4 ± 10.6	242.6 ± 39.1	142.3 ± 23.3	85.4 ± 13.5	84.2 ± 13.9	653.9 ± 66.4 (9.0)
P (rain)	0.4 ± 0.2 (1 %)	0.4 ± 0.2 (<1 %)	4.2 ± 1.8 (2 %)	6.6 ± 2.8 (5 %)	1.7 ± 0.8 (2 %)	2.2 ± 1.1 (3 %)	15.3 ± 5.4 (2 %) (3.0)
P (snow)	30.7 ± 5.3	68.0 ± 10.5	238.5 ± 38.7	135.7 ± 22.7	83.7 ± 13.2	82.0 ± 13.5	638.6 ± 65.0 (6.0)
Surface melt	57.2 ± 24.1	72.2 ± 33.8	101.0 ± 27.1	155.2 ± 48.4	67.4 ± 24.0	89.8 ± 33.2	542.9 ± 175.3 (121.7)
E + Su	15.7 ± 0.9	25.3 ± 1.6	16.8 ± 0.8	20.3 ± 1.7	16.4 ± 1.1	17.7 ± 0.9	112.2 ± 5.2 (1.8)
R	50.0 ± 22.7	62.6 ± 31.5	69.2 ± 21.0	112.6 ± 41.8	53.6 ± 19.4	70.0 ± 28.1	418.1 ± 151.1 (106.4)
Ablation (E + Su + R)	65.7 ± 22.6	87.9 ± 31.5	86.0 ± 21.4	132.9 ± 42.2	70.0 ± 19.9	87.7 ± 28.5	530.3 ± 153.0 (108.2)
Refreezing and retention (rain and surface melt minus runoff)	7.6 ± 2.8 (13 %)	10.0 ± 4.0 (14 %)	36.0 ± 8.9 (30 %)	49.2 ± 13.3 (30 %)	15.5 ± 6.1 (22 %)	22.0 ± 7.2 (24 %)	140.1 ± 35.5 (25 %) (18.3)
SMB	-34.6 ± 24.8	-19.6 ± 32.4	156.6 ± 44.5	9.3 ± 50.3	15.4 ± 23.6	-3.5 ± 32.1	123.7 ± 163.2 (-99.2)
2005–2014							
P	30.9 ± 5.1	71.0 ± 11.9	232.4 ± 25.2	138.5 ± 16.1	86.4 ± 8.6	85.3 ± 16.9	645.0 ± 39.0 (-5.1)
P (rain)	0.5 ± 0.3 (2 %)	0.4 ± 0.2 (<1 %)	5.2 ± 1.9 (2 %)	7.8 ± 2.3 (6 %)	2.0 ± 0.6 (2 %)	2.9 ± 1.3 (4 %)	18.7 ± 3.4 (3 %) (-2.8)
P (snow)	30.4 ± 5.0	70.6 ± 11.9	227.1 ± 25.0	130.8 ± 15.7	84.4 ± 8.6	82.9 ± 16.4	626.3 ± 39.2 (-2.3)
Surface melt	75.9 ± 26.9	101.7 ± 34.5	129.7 ± 16.3	202.4 ± 39.2	89.3 ± 19.7	124.6 ± 26.8	713.4 ± 138.6 (-79.7)
E + Su	15.7 ± 1.0	25.9 ± 1.1	17.3 ± 0.9	20.7 ± 1.5	16.7 ± 0.8	17.8 ± 0.9	114.1 ± 4.3 (-3.8)
R	67.6 ± 25.0	89.3 ± 31.0	91.7 ± 14.4	154.4 ± 36.3	71.2 ± 15.2	99.5 ± 22.4	573.7 ± 119.8 (-26.0)
Ablation (E + Su + R)	83.3 ± 24.7	115.2 ± 30.8	109.0 ± 14.2	175.1 ± 35.2	87.9 ± 15.0	117.3 ± 22.5	687.8 ± 118.8 (-29.8)
Refreezing and retention (rain and surface melt minus runoff)	8.8 ± 3.5 (12 %)	12.8 ± 5.3 (13 %)	43.3 ± 6.9 (32 %)	55.8 ± 12.1 (27 %)	20.1 ± 6.0 (22 %)	28.0 ± 8.1 (22 %)	158.4 ± 34.4 (22 %) (-56.6)
SMB	-52.4 ± 26.3	-44.2 ± 30.6	123.4 ± 35.7	-36.6 ± 45.0	-1.5 ± 16.4	-31.5 ± 29.7	-42.9 ± 133.5 (24.7)



1094 **Table 2:** Regional breakdown of GrIS specific runoff ($L s^{-1} km^{-2}$) and changes in specific runoff
1095 (linear; $L s^{-1} km^{-2} decade^{-1}$) for GrIS and each of the six individual sections both from 1979–
1096 2014 and 2005–2014. Changes in specific runoff are shown in the brackets.

1097

	N	NE	SE	SW	W	NW	GrIS
1979–2014	6.9 (1.6)	4.4 (1.5)	8.8 (1.9)	16.7 (4.1)	7.4 (1.8)	8.3 (2.1)	8.1 (2.0)
2005–2014	9.4 (-0.5)	6.2 (-1.0)	11.6 (-0.1)	22.9 (0.7)	9.8 (-0.5)	11.8 (1.5)	11.1 (-1.3)

1098